NASA/TM-2001-104606, Vol. 19

Technical Report Series on Global Modeling and Data Assimilation

Max J. Suarez, Editor

Volumn 19

A Thermal Infrared Radiation Parameterization for Atmospheric Studies

Ming-Dah Chou and Max J. Suarez
Goddard Space Flight Center
Greenbelt, Maryland

Xin-Zhong Liang
University of Illinois at Urbana-Champaign
Champaign, Illinois

Michael M.-H. Yan
Science Systems and Applications, Inc.
Lanham, Maryland

National Aeronautics and
Space Administration

Goddard Space Flight Center
Greenbelt, Maryland 20771

July 2001
Revised May 2003

ABSTRACT

This technical memorandum documents the longwave radiation parameterization developed at the Climate and Radiation Branch, NASA/Goddard Space Flight Center, for a wide variety of weather and climate applications. Based on the 1996-version of the Air Force Geophysical Laboratory HITRAN data base (Rothman et al., 1998), the parameterization includes the absorption due to major gaseous absorption (water vapor, CO_2, O_3) and most of the minor trace gases (N_2O, CH_4, *CFC's*), as well as clouds and aerosols. The thermal infrared spectrum is divided into nine bands. To achieve a high degree of accuracy and speed, various approaches of computing the transmission function are applied to different spectral bands and gases. The gaseous transmission function is computed either using the *k*-distribution method or the table look-up method. To include the effect of scattering due to clouds and aerosols, the optical thickness is scaled by the single-scattering albedo and asymmetry factor. The optical thickness, the single-scattering albedo, and the asymmetry factor of clouds are parameterized as functions of the ice and water content and the particle size. The parameterization can accurately compute fluxes to within 1% of the high spectral-resolution line-by-line calculations. The cooling rate can be accurately computed in the region extending from the surface to the 0.01-*hPa* level.

The computer code for this longwave parameterization is very easy to use. It has been implemented in atmospheric models for cloud, weather, and climate studies at many government institutes and universities. The code and sample calculations are accessible at *ftp://climate.gsfc.nasa.gov/pub/chou/clirad_lw/*

TABLE OF CONTENT

List of Figures

List of Tables

1. INTRODUCTION

Thermal infrared (or longwave, *LW*) radiation plays a crucial role in affecting weather, climate, and the sensitivity of climate to external radiative forcing. It is, therefore, important to have an accurate *LW* radiation parameterization in atmospheric models for weather and climate studies. In numerical model simulations of weather and climate, calculations of *LW* fluxes can easily take a third or more of the total computing time. As the spatial and temporal resolution of the models increases and the treatment of physical processes improves, it becomes clear that we need a fast and accurate *LW* radiation parameterization.

Detailed calculation of the *LW* fluxes involves three sets of integration: spectral integration, vertical integration, and directional integration. The spectral integration is the most time consuming, but it is the vertical integration that makes the parameterization for the *LW* radiation particularly difficult. If the atmosphere were vertically homogeneous in pressure and temperature, then the absorption coefficient would be a function only of wavenumber, and wavenumbers with the same absorption coefficient would be radiatively identical. The spectral integration could then be greatly simplified by using the *k*-distribution method (*c.f.* Arking and Grossman, 1972), in which only one set of radiative transfer calculations is needed for all the wavenumbers with the same absorption coefficient. In the real atmosphere, however, the dependence of the absorption coefficient on pressure and temperature varies with wavenumber, and in principle no two spectral intervals can be treated identically in the radiative transfer calculations. The difficulty is augmented by the narrowness of molecular absorption lines, which makes the absorption coefficient vary rapidly with wavenumber. Thus, it requires a very high spectral resolution to obtain spectrally integrated fluxes with high accuracy. To further complicate the flux calculations, there are numerous absorbers that have to be taken into account. Except for water vapor, those absorbers spread over the *LW* spectrum in narrow bands. The effects of those bands need to be computed individually.

At the Goddard Climate and Radiation Branch, we have developed various *LW* radiation parameterizations for the major water vapor, CO_2 and O_3 absorption bands (Chou and Kouvaris, 1991; Chou et al., 1993). These IR radiation parameterizations have been shown to be accurate and efficient in computing cooling rate not only in the troposphere and lower stratosphere, but also in the middle atmosphere (up to the 0.01-*hPa* level). The code was documented in a *NASA Technical Memorandum* (Chou and Suarez, 1994).

This technical memorandum is an extension of Chou and Suarez (1994) by including the absorption due to minor trace gases of N_2O, CH_4, and *CFC's* (Kratz et al., 1998) and parameterizations for the absorption and scattering due to clouds (Chou et al., 1999). Aerosols are also included, but with optical properties specified as input parameters. This *LW* radiation code has been implemented in the Goddard general circulation models (Bacmeister and Suarez,, 2001; Sud and Mocko, 1999) and the cloud ensemble model (Tao et al., 2001). It has also been used at various universities and government institutes.

2. INFRARED TRANSFER EQUATIONS

Let us consider a thin atmospheric layer at pressure p' with a temperature θ', which has a differential pressure thickness dp' and an optical thickness $d\tau_\nu$ at wavenumber ν (Figure 1). The radiance emitted by this layer is $R_\nu(\theta')d\tau_\nu/\mu$, where μ is the cosine of the angle between the beam and the vertical, and R_ν is the Planck function. Let us further consider a lower level at pressure p at which we wish to compute the downwelling flux, and let us assume that between p and p' there is a mixture of gaseous, cloud, and aerosol absorbers with monochromatic optical thickness $\tau_\nu(p,p')$. The transmittance between p' and p in the direction μ is $e^{-\tau_\nu(p,p')/\mu}$. When scattering is neglected, the contribution of the layer between p' and $p'+dp'$ to the *radiance* at the level p is then given by

$$dI_\nu^{\downarrow}(\mu) = R_\nu(\theta')\frac{d\tau_\nu}{\mu}e^{-\tau_\nu(p,p')/\mu} \tag{2.1}$$

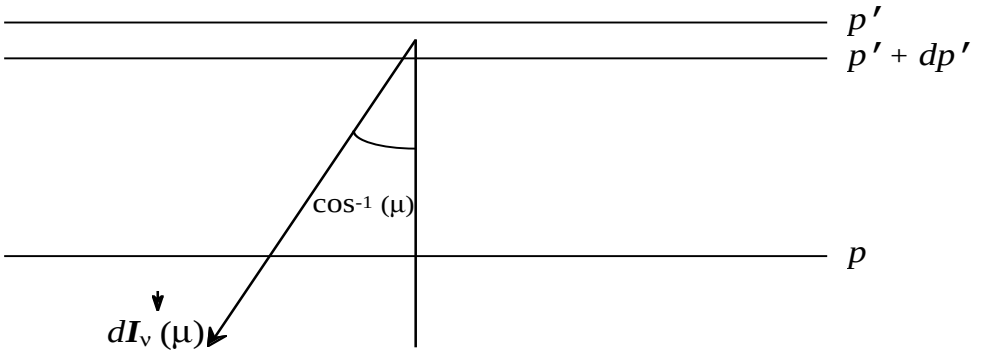

Figure 1. Contribution from a differential layer at p' to the downward radiance at p.

The contribution of the layer to the downward *flux* at p can be derived by angular integration of (2.1) over the hemisphere,

$$\begin{aligned} dF_\nu^{\downarrow} &= 2\pi \int_0^1 dI_\nu^{\downarrow}(\mu)\mu d\mu \\ &= 2\pi R_\nu(\theta') \int_0^1 \frac{d\tau_\nu}{\mu} e^{-\tau_\nu(p,p')/\mu} \mu d\mu \\ &= -B_\nu(\theta') dT_\nu(p,p') \end{aligned} \tag{2.2}$$

where $B_\nu(\theta) = \pi R_\nu(\theta)$ is the Planck flux, and $T_\nu(p,p')$ is the flux transmittance for isotropic radiation given by

$$T_\nu(p,p') = 2\int_0^1 e^{-\tau_\nu(p,p')/\mu} \mu d\mu \tag{2.3}$$

The total downward flux integrated over heights and wavenumbers is then given by

$$F^{\downarrow}(p) = \int d\nu \left\{ \int_0^p B_\nu(\theta') \frac{\partial T_\nu(p,p')}{\partial p'} dp' \right\} \tag{2.4}$$

Similarly, the upward flux can be expressed as

$$F^{\uparrow}(p) = \int d\nu \left\{ \begin{aligned} &\left[\varepsilon_\nu B_\nu(\theta_s) + (1-\varepsilon_\nu) F_\nu^{\downarrow}(p_s) \right] T_\nu(p,p_s) \\ &+ \int_{p_s}^p B_\nu(\theta') \frac{\partial T_\nu(p,p')}{\partial p'} dp' \end{aligned} \right\} \tag{2.5}$$

where ε_ν is the surface emissivity, p_s is the surface pressure, and θ_s is the Earth's surface skin temperature. Finally, the cooling rate is given by

$$-\frac{\partial \theta(p)}{\partial t} = \frac{1}{c_p g} \frac{\partial}{\partial p} \left[F^{\downarrow}(p) - F^{\uparrow}(p) \right] \tag{2.6}$$

where c_p is the heat capacity of air at constant pressure, and g is the gravitational acceleration.

3. SPECTRAL BANDS

3.1 The 10 Bands

For computing thermal IR fluxes, the spectrum is divided into 9 bands and a subband. Table 1 shows the spectral ranges for these 10 bands, together with the absorbers involved in each band. The water vapor line absorption covers the entire IR spectrum, while the water vapor continuum absorption is included in the 540-1380 cm^{-1} spectral region. The absorption due to CO_2 is included in the 540-800 cm^{-1} region, and the absorption due to O_3 is included in the 980-1100 cm^{-1} region. The minor absorption due to CH_4, N_2O, *CFC's*, and CO_2 is scattered between 800 cm^{-1} and 1380 cm^{-1} region in Bands 4-7. The absorption due to N_2O in the 17-μm region is included in Sub-band 3a and is identified as Band 10.

3.2 Planck-Weighted Band Integrals

From (2.4) and (2.5), the downward and upward fluxes integrated over a spectral band *i* can be written as

$$F_i^{\downarrow}(p) = \int_0^p B_i(\theta')\left(\frac{\partial T(p,p')}{\partial p'}\right)_i dp' \tag{3.1}$$

$$\begin{aligned} F_i^{\uparrow}(p) = {} & \varepsilon_i B_i(\theta_s) T_i(p,p_s) + \int_{p_s}^p B_i(\theta')\left(\frac{\partial T_i(p,p')}{\partial p'}\right)_i dp' \\ & + (1-\varepsilon_i) F_i^{\downarrow}(p_s) T_i(p,p_s) \end{aligned} \tag{3.2}$$

where

$$F_i(p) = \int_{\Delta\nu_i} F_\nu(p) d\nu \tag{3.3}$$

$$B_i(\theta) = \int_{\Delta\nu_i} B_\nu(\theta) d\nu \tag{3.4}$$

$$T_i(p,p') = \frac{1}{B_i(\theta')} \int_{\Delta\nu_i} B_\nu(\theta') T_\nu(p,p') d\nu \tag{3.5}$$

Table 1. Spectral bands, absorbers, and transmittance parameterizations.

Band	Spectral Range (cm^{-1})	Absorber	Options for Transmittance Parameterization	
			"LOW"	"HIGH"
1	0-340	H_2O line	*K*	*T*
2	340-540	H_2O line	*K*	*T*
3a	540-620	H_2O line	*K*	*T*
3b	620-720	H_2O continuum	*C*	*C*
3c	720-800	CO_2	*K*	*T*
4	800-980	H_2O line	*K*	*K*
		H_2O continuum	*C*	*C*
		CO_2, F11, F12, F22	*K*	*K*
5	980-1100	H_2O line, CO_2, F11	*K*	*K*
		H_2O continuum	*C*	*C*
		O_3	*T*	*T*
6	1100-1215	H_2O line	*K*	*K*
		H_2O continuum	*C*	*C*
		H_2O, CH_4, F12, F22	*K*	*K*
7	1215-1380	H_2O line, N_2O, CH_4	*K*	*K*
		H_2O continuum	*C*	*C*
8	1380-1900	H_2O line	*K*	*T*
9	1900-3000	H_2O line	*K*	*K*
10	540-620	H_2O line, CO_2, N_2O	*K*	*K*
		H_2O continuum	*C*	*C*

K: k-distribution method with linear pressure scaling.

T: Table look-up with temperature and pressure scaling.

C: One-parameter temperature scaling for water vapor continuum absorption.

$$\left(\frac{\partial T(p,p')}{\partial p'}\right)_i = \frac{1}{B_i(\theta')}\int_{\Delta\nu_i} B_\nu(\theta')\frac{\partial T_\nu(p,p')}{\partial p'}d\nu \tag{3.6}$$

are the Planck-weighted band integrals, and $\Delta\nu_i$ is the width of the i^{th} band.

Within each spectral band, either the range of B_ν is sufficiently small or the shape of B_ν is sufficiently independent of temperature that we can make the following approximation

$$T_i(p,p') \approx \frac{1}{B_i(\theta_o)}\int_{\Delta\nu_i} B_\nu(\theta_o)T_\nu(p,p')d\nu \tag{3.7}$$

$$\left(\frac{\partial T(p,p')}{\partial p'}\right)_i \approx \frac{1}{B_i(\theta_o)}\int_{\Delta\nu_i} B_\nu(\theta_o)\frac{\partial T_\nu(p,p')}{\partial p'}d\nu = \frac{\partial T_i(p,p')}{\partial p'} \tag{3.8}$$

where θ_o is a typical value of the atmospheric temperatures, which is set to be $250K$.

With the approximation (3.7) and (3.8), the band-integrated fluxes reduce to

$$F_i^{\downarrow}(p) = \int_0^p B_i(\theta')\frac{\partial T_i(p,p')}{\partial p'}dp' \tag{3.9}$$

$$\begin{aligned} F_i^{\uparrow}(p) = {} & \varepsilon_i B_i(\theta_s)T_i(p,p_s) + \int_{p_s}^p B_i(\theta')\frac{\partial T_i(p,p')}{\partial p'}dp' \\ & + (1-\varepsilon_i)F_i^{\downarrow}(p_s)T_i(p,p_s) \end{aligned} \tag{3.10}$$

3.3 Band-Integrated Planck Functions

The spectrally integrated Planck fluxes were pre-computed for each band and then fit by a 5^{th}-degree polynomial in temperature,

$$B_i(\theta) = c_{i,0} + \sum_{n=1}^{5} c_{i,n}\theta^n \tag{3.11}$$

When integrated over all bands, errors in this regression are negligible (< 0.1%) for $150K < \theta < 350K$. The coefficients *c's* are listed in Table 2.

Table 2. Coefficients for computing the spectrally integrated Planck flux from Equation (3.11). Units of θ in (3.11) are *Kelvin*.

Band	c_0	c_1	c_2	c_3	c_4	c_5
1	5.344e+0	-2.062e-1	2.533e-3	-6.863e-6	1.012e-8	-6.267e-12
2	2.715e+1	-5.404e-1	2.950e-3	2.723e-7	-9.338e-9	9.968e-12
3	-3.486e+1	1.113e+0	-1.301e-2	6.496e-5	-1.182e-7	8.042e-11
4	-6.051e+1	1.409e+0	-1.208e-2	4.405e-5	-5.674e-8	2.566e-11
5	-2.669e+1	5.283e-1	-3.445e-3	6.072e-6	1.252e-8	-2.155e-11
6	-6.727e+0	4.226e-2	1.044e-3	-1.292e-5	4.740e-8	-4.486e-11
7	1.879e+1	-5.836e-1	6.968e-3	-3.939e-5	1.012e-7	-8.230e-11
8	1.034e+2	-2.513e+0	2.375e-2	-1.069e-4	2.184e-7	-1.370e-10
9	-1.048e+1	3.821e-1	-5.227e-3	3.441e-5	-1.108e-7	1.409e-10
10	1.677e+0	6.540e-2	-1.813e-3	1.291e-5	-2.672e-8	1.979e-11

3.4 Sensitivity of Upward Flux to Surface Temperature

The parameterization also computes the sensitivity of upward fluxes at all levels to the surface temperature θ_s. In a general circulation model, the *LW* parameterization is called relatively infrequently (every few hours), whereas the boundary layer and land surface parameterizations use time steps of a few minutes. To maintain consistency between the upward radiative fluxes aloft and that at the surface when the surface temperature changes significantly between calls to the *LW* parameterization, all fluxes are linearized about the surface temperature at the beginning of the radiation interval, and radiative heating rates are recomputed based on this linearization every few minutes, at each time step. The partial derivative of the upward flux with respect to the surface temperature is computed from

$$\frac{\partial F_i^{\uparrow}(p)}{\partial \theta_s} = T_i(p, p_s)\left[\frac{\varepsilon_i \partial B_i(\theta)}{\partial \theta}\right]_{\theta=\theta_s} = T_i(p, p_s)\varepsilon_i\left[c_{i,1} + \sum_{n=2}^{5} n c_{i,n}\theta_s^{\,n-1}\right] \tag{3.12}$$

4. BAND-AVERAGED TRANSMISSION FUNCTIONS OF GASES

For accuracy and speed considerations, the flux transmittance defined by (3.7) is computed using three different approaches, depending on the absorber and the spectral band:

- The *k*-distribution method with linear pressure scaling is applied to the absorption due to water vapor and minor trace gases. This method is also applied to the CO_2 absorption in Band 3 if accurate cooling rate calculations in the middle atmosphere ($p < 10\ hPa$) are not required.

- The transmittances due to CO_2 and O_3 absorption in Bands 3 and 5 are obtained from pre-computed transmittance tables. Because the *k*-distribution method with linear pressure scaling underestimates the water vapor cooling rate in the middle atmosphere, the transmittances of the three strongest water vapor absorption bands (Bands 1, 2 and 8) are also derived from pre-computed transmittance tables if accurate computations of the water vapor cooling in the middle atmosphere are required.

- The transmittances due to water vapor continuum absorption in Bands 3-7 are computed using a one-parameter scaling approach.

Applications of these parameterizations to the different spectral bands and absorbers are summarized in Table 1.

4.1 The k-distribution method

As shown in Chou et al. (1993), the cooling due to water vapor in the lower atmosphere ($p > 10\ hPa$) is primarily attributable to the spectral regions away from the center of absorption lines. The absorption coefficient is approximately linear in pressure, and its dependence on temperature varies smoothly with wavenumber. Under these conditions, the absorption coefficient at any temperature and pressure is simply proportional to its value at a reference pressure and temperature. The absorption coefficient can, therefore, be extrapolated from the absorption coefficient at a reference pressure and temperature according to

$$k_\nu(p, \theta) = k_\nu(p_r, \theta_r)\,(p / p_r)^m\, h(\theta, \theta_r) \tag{4.1}$$

where p_r and θ_r are the reference pressure and temperature, m is an empirical constant, and $h(\theta, \theta_r)$ is the temperature scaling factor, which we fit by

$$h(\theta, \theta_r)=1+\alpha(\theta-\theta_r)+\beta(\theta-\theta_r)^2 \quad (4.2)$$

The regression coefficients α and β are derived for each spectral band to minimize errors in flux transmittances. Details of the derivation of the coefficients α and β are given in Chou et al. (1993). Values of p_r, θ_r, m, α, and β are given in Table 3 for scaling the water vapor and CO_2 absorption coefficient.

Table 3. Spectral bands, reference pressure and temperature, and the coefficients for the pressure and temperature scaling used in the *k*-distribution method. Band 3 is divided into three sub-bands.

Band	H_2O p_r = 500 *hPa* θ_r = 250 *K*			CO_2 θ_r = 250 *K*			
	m	$\alpha(K^{-1})$	$\beta(K^{-2})$	p_r (*hPa*)	m	$\alpha(K^{-1})$	$\beta(K^{-2})$
1	1.0	.0021	-1.01e-5				
2	1.0	.0140	5.57e-5				
3a	1.0	.0167	8.54e-5	300	0.50	.0179	1.02e-4
3b	1.0	.0167	8.54e-5	30	0.85	.0042	2.00e-5
3c	1.0	.0167	8.54e-5	300	0.50	.0184	1.12e-4
4	1.0	.0302	2.96e-4				
5	1.0	.0307	2.86e-4				
6	0.77	.0195	1.11e-4				
7	0.5	.0152	7.61e-5				
8	1.0	.0008	-3.52e-6				
9	1.0	.0096	1.64e-5				
10	1.0	.0149	6.20e-5	300	0.50	.0179	1.02e-4

With the scaling of (4.1), the monochromatic flux transmittance (2.3) can be expressed as

$$T_\nu(p,p') = 2\int_0^1 e^{-k_\nu(p_r,\theta_r)w(p,p')/\mu}\,\mu d\mu \tag{4.3}$$

where *w* is the scaled absorber amount given by

$$w(p,p') = \frac{1}{g}\int_{p'}^{p} c(p'')(p''/p_r)^m h(\theta'';\theta_r)dp'' \tag{4.4}$$

and *c* is the absorber mass concentration. It can be seen from (4.3) and (4.4) that the dependence of T_ν on wavenumber is separated from its dependence on pressure and temperature. Wavenumbers which have the same absorption coefficient at p_r and θ_r will have the same transmittance at all other pressures and temperatures. Within a narrow spectral interval where the Planck function can be considered constant, these wavenumbers are radiatively identical, and the integration over wavenumber can be replaced by an integration over the absorption coefficient *k*,

$$\int_{\Delta\nu}(\quad)d\nu/\Delta\nu = \int_0^\infty(\quad)f(k)dk \tag{4.5}$$

where *f(k)* is the *k*-distribution function *at the reference pressure* p_r *and temperature* θ_r, and

$$\int_0^\infty f(k)dk = 1 \tag{4.6}$$

This is the basic assumption of the *k*-distribution method. It should be noticed that the approximation for relating the absorption coefficient at a pressure level to that at other levels, as shown in (4.1), is different from the *correlated-k distribution* method (e.g. Wang and Shi, 1988; Goody et al., 1989; Lacis and Oinas, 1991; Fu and Liou, 1992; Mlawer et al., 1997). However, it is also a type of the correlated-*k* approximation with a well-defined correlation.

If we divide a wide spectral band into a number of narrow sub-bands, for which the Planck function can be considered constant, and apply the *k*-distribution method to each sub-band, the Planck-weighted transmission function given by (3.7) becomes

$$T(w) = \frac{\sum_j \left[B_j(\theta_o) \int_{\delta\nu_j} T_\nu(w) d\nu \right]}{B(\theta_o)} = \frac{\sum_j \left[B_j(\theta_o) \delta\nu_j \int_k T_k(w) f_j(k) dk \right]}{B(\theta_o)} \tag{4.7}$$

where

$$T_k(w) = 2\int_0^1 e^{-kw/\mu} \mu d\mu \tag{4.8}$$

$B_j(\theta_o)$ is the mean Planck function of the sub-band j, and $f_j(k)$ is the k-distribution function of the sub-band at the reference pressure p_r and temperature θ_r.

The flux transmittance given by (4.8) can be accurately computed by using the following approximation (see Figure 5b of Chou and Arking, 1980)

$$T_k(w) \approx e^{-kw/\bar{\mu}} \tag{4.9}$$

where $1/\bar{\mu}$ is the diffusivity factor taken to be 1.66. Using this approximation and replacing the k integral by a simple quadrate, Equation (4.7) reduces to

$$T(w) = \sum_{n=1}^{N} e^{-k_n w/\bar{\mu}} \Delta g_n \tag{4.10}$$

where Δg_n is the Planck-weighted k-distribution function for the n^{th} k-interval given by

$$\Delta g_n = \sum_j f_j(k_n) \delta k_n \frac{B_j(\theta_o)}{B(\theta_o)} \delta\nu_j \tag{4.11}$$

Values of Δg_n are first derived from line-by-line calculations and then slightly adjusted using regression so that the *rms* difference between the transmittances computed from the *line-by-line* method and from (4.10) is minimized. (The *line-by-line* calculations are briefly discussed in Section Section 9). The adjustment is necessary because of the small number of terms (N = 6) used and the diffusivity (4.9) approximation applied. Details are given in Chou et al. (1993).

Calculations of the Planck-weighted flux transmission function using (4.10) are very fast for two reasons: (1) For each k, it requires only L exponential operations for calculating $e^{-k\Delta w_l/\bar{\mu}}$, l =1, 2,...., L, where L is the total number of atmospheric layers, and Δw_l is the scaled absorber amount in the layer l. The transmittance of a path consisting of more than one layer can be obtained by multiplying the transmittances of individual layers. By comparison, the commonly used band model require at least 0.5 L^2 exponential operations. (2) We choose values of k in such a way that

$$k_n = \eta k_{n-1} \qquad n=2, 3, \ldots, N \qquad (4.12)$$

where η is a positive integer. With this choice of k's, only a single set of L exponential operations for the first value of k is needed. The other exponential terms can be derived from that of the previous value of k, with each derivation involving only ~3 multiplication operations. Because a multiplication operation is much faster than an exponential operation, flux calculations can be greatly accelerated by choosing values of k's according to (4.12) for computing transmittances. The first absorption coefficient, k_1, the constant η, and the k -distribution function are given in Table 4 for the water vapor.

Table 4. Parameters for the transmittance given by (4.10) due to water vapor line absorption. $k_1/\bar{\mu}$ is the first absorption coefficient, and η is the constant given in (4.12). Δg is the k-distribution function (4.11). Band 3 is treated separately in Section 4.5. Units of k are $g^{-1}\,cm^2$.

	Band 1	Band 2	Band 4	Band 5	Band 6	Band 7	Band 8	Band 9	Band 10
$k_1/\bar{\mu}$	2.96e+1	4.17e-1	5.25e-4	5.25e-4	9.37e-3	4.72e-2	1.32e+0	5.25e-4	1.06e-1
η	6	6	6	6	8	9	6	16	8
Δg_1	.2747	.1521	.4654	.5543	.5955	.1958	.0740	.1437	.3153
Δg_2	.2717	.3974	.2991	.2723	.2693	.3469	.1636	.2197	.4604
Δg_3	.2752	.1778	.1343	.1131	.0953	.3147	.4174	.3185	.1326
Δg_4	.1177	.1826	.0646	.0443	.0335	.1013	.1783	.2351	.0798
Δg_5	.0352	.0374	.0226	.0160	.0064	.0365	.1101	.0647	.0119
Δg_6	.0255	.0527	.0140	.0000	.0000	.0048	.0566	.0183	.0000

MINOR ABSORPTION BAND

In addition to the major absorption due to water vapor, CO_2 and O_3, there are also many weak absorption bands of N_2O, CH_4, CO_2, and *CFC*'s located mostly in the water vapor window region between 800 and 1300 cm^{-1}. Individually, the effect of these bands on fluxes is small, but collectively the effect is to reduce the outgoing LW radiation at the top of a clear atmosphere by ~4 $W\ m^{-2}$ and to enhance the surface heating by ~2 $W\ m^{-2}$. These effects are significant in the study of anthropogenic climate change.

The spectral bands which include the minor absorption are shown in Table 1. A total of 13 sets of minor transmission functions are computed: four in Band 4, two in Band 5, four in Band 6, two in Band 7, and one in Band 10 (Sub-band 3a).

The *k*-distribution method is also applied to computing the transmission functions averaged over individual minor spectral bands (Table 1). The reference pressure and temperature, values of the parameters used for the minor bands are listed in Tables 5-7 (see Kratz et al., 1993, and Kratz et al., 1998, for details of the parameterization). Because the absorption is weak in those minor bands, it requires only a small number (1-4) of the *k*-intervals for accurate transmission calculations.

Table 5. Parameters for computing the *flux* transmission functions due to N_2O and CH_4 using the *k*-distribution method. ($p_r = 500\ hPa$ and $\theta_r = 250\ K$).

	N_2O			CH_4	
	Band 6	Band 7	Band 10	Band 6	Band 7
k_1 / μ	6.32e-2	5.36e-2	2.52e-1	5.81e-3	6.29e-2
η	21	8	58		12
Δg_1	.9404	.5620	.971	1.000	.6107
Δg_2	.0596	.1387	.029		.2802
Δg_3		.2406			.1073
Δg_4		.0587			.0018
m	.0	.48	.0	.0	.65
α	1.93e-3	1.38e-3	1.45e-3	1.70e-2	5.96e-4
β	4.38e-6	7.48e-6	3.67e-6	1.58e-4	-2.29e-6

Table 6. Same as Table 5, except for the absorption due to CO_2.

	Band 4	Band 5	Band 10*
k_1 / μ	1.92e-7	1.92e-7	2.66e-5
η	5	5	8
Δg_1	.1216	.0687	.267
Δg_2	.2436	.1480	.220
Δg_3	.2498	.1951	.210
Δg_4	.2642	.3344	.241
Δg_5	.0781	.1720	.020
Δg_6	.0427	.0818	.042
m	.0	.0	.5
α	3.58e-2	3.43e-2	1.79e-2
β	4.05e-4	3.74e-4	1.02e-4

* $p_r = 300\ hPa$.

Table 7. Same as Table 5, except for the minor CFC absorption bands. There is only one *k*-interval for each CFC band, and there is no pressure scaling applied, i.e. *m=0*.

	CFC-11		*CFC-12*		*CFC-22*	
	Band 4	Band 5	Band 4	Band 6	Band 4	Band 6
$\frac{k_1}{\mu}$	1.90e+1	1.02e+1	1.58e+1	3.70e+1	6.18e+0	3.28e+1
α	1.27e-3	8.19e-4	8.77e-4	8.62e-4	9.65e-4	-3.00e-5
β	3.56e-6	4.68e-6	-5.88e-6	-4.23e-6	1.31e-5	5.25e-7

4.2 Pre-computed Transmission Tables

Although the *k*-distribution method with linear pressure scaling is computationally very fast, it is not accurate in the middle atmosphere (0.01-10 *hPa*), where the pressure ranges by 3 orders of magnitude and where the Doppler broadening of absorption lines is important. Cooling in the middle atmosphere is primarily due to CO_2 in the 15-μm band (Band 3), O_3 in the 9.6-μm band (Band 5) and secondarily due to water vapor near the centers of absorption bands (Bands 1, 2, and 8).

It is shown in Chou and Kouvaris (1991) and Chou and Suarez (1994) that transmittances in these bands can be simply derived from pre-computed transmission tables. The basis for this method is that a nonhomogenous layer with pressure and temperature varying with height can be treated as if it were homogeneous with an effective pressure and temperature defined by

$$p_{eff} = \frac{\int p du}{\int du} \tag{4.13}$$

$$\theta_{eff} = \frac{\int \theta du}{\int du} \tag{4.14}$$

where u is the absorber amount, and the integration is over the depth of a layer. It has been well recognized (e.g. Wu, 1980; Chou and Kouvaris, 1991) that the contribution to the atmospheric cooling is primarily from near-by layers. The pressure and temperature variations among near-by layers are small, and the simple scaling approximations of (4.13) and (4.14) can be applied to accurate calculations of cooling rate.

With the two-parameter scaling of (4.13) and (4.14), the flux transmission becomes a function of the absorber amount and the effective temperature and pressure. These dependencies can be accurately pre-computed from the following equation using a line-by-line method,

$$T(u, p_{eff}, \theta_{eff}) = \frac{\int_{\Delta\nu} T_\nu(u, p_{eff}, \theta_{eff}) B_\nu(\theta_o) d\nu}{\int_{\Delta\nu} B_\nu(\theta_o) d\nu} \tag{4.15}$$

where $\Delta\nu$ is the width of the entire spectral band. The band transmission varies rapidly with pressure, but rather smoothly with temperature. The size of the three-dimensional transmission tables can be reduced to three two-dimensional tables using a quadratic fit in temperature,

$$T(u, p_{eff}, \theta_{eff}) = a(u, p_{eff}) + b(u, p_{eff})(\theta_{eff} - 250) + c(u, p_{eff})(\theta_{eff} - 250)^2 \tag{4.16}$$

where a, b, and c are regression coefficients. This regression is valid for temperatures ranging from $170K$ to $330K$; for this range it introduces only ~ 1% error in the absorptance. Table 8 shows the first values, the intervals, and the interval numbers of $log_{10}(u)$ and $log_{10}(p_{eff})$ of the tables a, b and c for transmissions due to CO_2 absorption in the 15 μm region, O_3 absorption in the 9.6 μm region, and water vapor absorption in the three strong absorption bands. It is noticed that the transmission tables can be applied to an atmosphere with a CO_2 concentration 100 times of the present value, *i.e.* 35000 *ppmv*.

The absorption due to O_3 covers a spectral range wider than that of Band 5 shown in Table 1. To include the weak absorption outside this spectral band, we have made adjustment to the transmission function by requiring that

$$(1-\bar{\tau})\int_{\nu_1}^{\nu_2} B_\nu(T) d\nu = \int_{\nu_a}^{\nu_b} (1-\tau_\nu) B_\nu(T) d\nu \tag{4.17}$$

Table 8. The first values, $log_{10}(w_{eff})_1$ and $log_{10}(p_{eff})_1$, the intervals, $\Delta log_{10}(w_{eff})$ and $\Delta log_{10}(p_{eff})$, and the numbers, *nw* and *np*, of $log_{10}(w_{eff})$ and $log_{10}(p_{eff})$ of the tables *a*, *b* and *c* for transmittance calculations using (4.16). Units of w_{eff} are $g\ cm^{-2}$ for water vapor and $(cm\text{-}atm)_{STP}$ for CO_2 and O_3, and the unit of p_{eff} is *hPa*.

	Band 1	Band 2	Band 3	Band 5	Band 8
Absorber	H_2O	H_2O	CO_2	O_3	H_2O
$log_{10}(w_{eff})_1$	-8	-8	-4	-6	-8
$log_{10}(p_{eff})_1$	-2	-2	-2	-2	-2
$\Delta log_{10}(w_{eff})$	0.3	0.3	0.3	0.3	0.3
$\Delta log_{10}(p_{eff})$	0.2	0.2	0.2	0.2	0.2
nw	31	31	30	21	31
np	26	26	26	26	26

where ν_1 - ν_2 is the spectral range of Band 5, ν_a - ν_b is a wider spectral range that covers all the molecular lines in the absorption band, and $\bar{\tau}$ is the effective mean transmission of Band 5. Thus, $\bar{\tau}$ includes the effect of the O_3 absorption outside the spectral range ν_a - ν_b. We could have expanded the range ν_1 - ν_2, but the accuracy of the transmission calculations would be reduced when (4.27) is applied to include the water vapor effect, which is discussed in Section 4.4. The adjusted mean transmission is then pre-calculated from

$$\bar{\tau} = 1 - \frac{\int_{\nu_a}^{\nu_b} (1-\tau_\nu) B_\nu(T) d\nu}{\int_{\nu_1}^{\nu_2} B_\nu(T) d\nu} \tag{4.18}$$

The method of table look-up is simple and accurate. As shown in Chou and Kouvaris (1991) and Chou and Suarez (1994), it can be applied to accurate calculating the fluxes and cooling rate in both the middle and lower atmosphere extending from 0.01 *hPa* to the earth's surface. However, this method could be significantly slower than the *k*-distribution method on computers that cannot efficiently perform table look-ups. We have therefore provided the option

of using the *k*-distribution method for all bands, except for the computation of O_3 transmission in Band 5.

4.3 One-parameter scaling for water vapor continuum absorption

Water vapor continuum absorption is included in Bands 2-7. The water vapor continuum absorption coefficient increases with increasing water vapor partial pressure but with decreasing temperature. It can be approximated by

$$k_\nu(p_e,\theta) = k_{\nu,o}\left(\frac{p_e}{p_o}\right) e^{1800\left(\frac{1}{\theta}-\frac{1}{296}\right)} \tag{4.19}$$

where p_e is the water vapor partial pressure in hPa, p_o = 1013 hPa, and $k_{\nu,o}$ is the absorption coefficient when p_e = 1013 hPa and θ = 296K. Values of $k_{\nu,o}$ comes from two sources: one from the analytical representation given by Roberts et al. (1976) which is a fit to the laboratory data of D. E. Burch and the other from Version CKD-2.3 of Clough et al. (1989).

With the scaling of (4.19) for the absorption coefficient, the flux transmission reduces to

$$T_\nu(p,p') = 2\int_0^1 e^{-k_{\nu,o}w^c(p,p')/\mu}\,\mu d\mu \tag{4.20}$$

where w^c is the scaled water vapor amount for continuum absorption given by

$$w^c(p,p') = \frac{1.61}{g}\int_{p'}^{p}\left(\frac{p''}{p_o}\right) q^2(p'') e^{1800\left[\frac{1}{\theta(p'')}-\frac{1}{296}\right]} dp'' \tag{4.21}$$

Here we have used the approximation

$$p_e \approx \frac{q\,p}{0.622} \tag{4.22}$$

and q is the specific humidity.

Taking the Planck-weighted average of (4.20) over a band we have

$$T(w^c) = \frac{\int_{\Delta\nu} T_\nu\left(w^c\right) B_\nu(\theta_o)\,d\nu}{\int_{\Delta\nu} B_\nu(\theta_o)\,d\nu} \tag{4.23}$$

where we note that the transmission is a function of w^c only. The absorption coefficient $k_{v,o}$ varies slowly with wavenumber, except in Band 3 where it varies by a factor of ≈3.5. Therefore, we divide Band 3 into three sub-bands (see Section 4.5 for more detail of the division of Band 3 into 3 subbands). The Planck-weighted flux transmissions for the three sub-bands and for Bands 4 - 7 were computed from (4.23). These transmittances were then fit by

$$T(w^c) \approx e^{-k^c w^c / \overline{\mu}} \tag{4.24}$$

Two sets of the effective absorption coefficients, $k^c / \overline{\mu}$, are derived based on Robert et al. and Clough et al. They are given in Table 9.

Table 9. The effective absorption coefficient $k^c / \overline{\mu}$ for the water vapor continuum absorption for Bands 1-7. Units of $k^c / \overline{\mu}$ are $g^{-1}\ cm^2$.

	Band1	*Band2*	*Band 3a*	*Band 3b*	*Band 3c*	*Band 4*	*Band 5*	*Band 6*	*Band 7*
Roberts	1790	339	109.6	54.8	27.4	15.8	9.40	7.75	7.70
Clough	1610	271	91.2	49.6	30.3	16.8	8.31	6.52	12.7

Differences in cooling rate and flux calculations using these two sets of data are very small. The left panel of the figure given below shows the cooling rate profiles using the Roberts et al. data (solid curve) and the Clough et al. data (dashed curve) for a typical clear-sky tropical atmosphere. Also shown in the figure are the net upward fluxes at the top of the atmosphere (TOA) and the surface (SFC). The flux difference is very small, < 0.5 W m^{-2}.

The continuum absorption coefficient is very large in Band 1 and Band 8 (not shown in the table), but the effects on the cooling rate and fluxes are negligible due to overlapping with the strong absorption near line centers. In our previous code, the continuum absorption was not included in Band 2. The solid curve in the right panel of the figure shows the cooling profile with the continuum absorption included in Bands 2-7. The dashed curve is the same except the continuum absorption is not included in Band 2. It can be seen that the use of the current code, which includes Band 2, has an effect of increasing the cooling in the middle troposphere and decreasing the cooling in the lower troposphere by 0.2-0.3˚C day^{-1}.

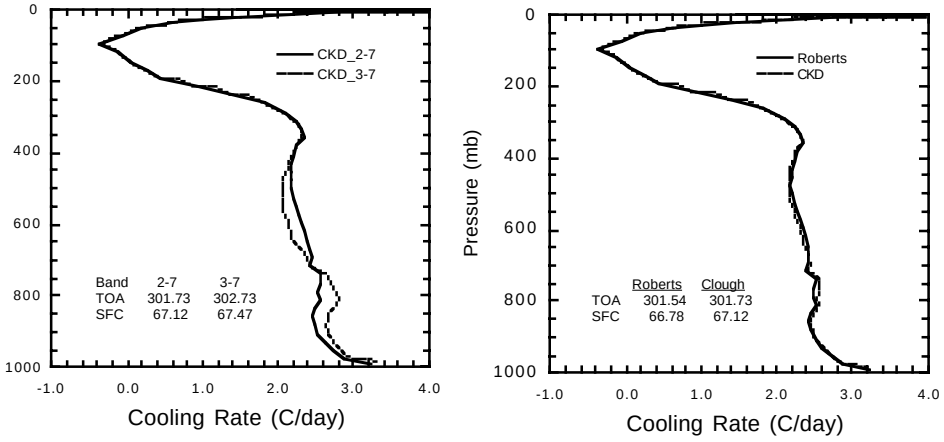

4.4 Overlapping of Gaseous Absorptions

When there are more than one absorber involved in a spectral band, overlaps must be considered. The total transmission for, say, two absorbers, can be written as

$$T_{12} = \frac{\int T_1(\nu) T_2(\nu) d\nu}{\int d\nu} \tag{4.25}$$

where the subscripts 1 and 2 denote the two absorbers. If the transmittance is expressed as the sum of the mean over the spectral band, $\overline{T}$, and the deviation from the mean, T', then (4.25) reduces to

$$T_{12} = \frac{\int \left(\overline{T_1} + T'_1(\nu)\right)\left(\overline{T_2} + T'_2(\nu)\right) d\nu}{\int d\nu} = \overline{T_1}\,\overline{T_2} + \frac{\int T'_1(\nu) T'_2(\nu) d\nu}{\int d\nu} \tag{4.26}$$

If the overall shapes of the absorption curves due to both absorbers are uncorrelated, the last term of (4.26) can be neglected, and the total transmittance becomes

$$T_{12} = \overline{T}_1 \overline{T}_2 \tag{4.27}$$

4.5 Special Treatment of the 15-μm Band

The 15-μm band poses additional difficulties for two reasons. First, the water vapor line absorption and the continuum absorption are highly correlated. As can be seen in the bottom two panels of Figure 2, the absorption coefficient increases with decreasing wavenumber by a factor of about 100 for water vapor line absorption and about 10 for continuum absorption. Thus, the water vapor line and continuum absorption are highly correlated, and the approximation (4.27) cannot be applied directly to the entire band. Second, the CO_2 absorption coefficients differ by several orders of magnitude between the band center and the wings (see the top panel of Figure 2). Rather than trying to parameterize the correlation effect or the variations in CO_2 absorption, we simply divide the band into three sub-bands (see the bottom panel of Figure 2 and Table 1) and then combine the parameterized transmittances of the sub-bands into a single band transmittance. This transmittance is then used in the usual way to solve the transfer equations for the entire band.

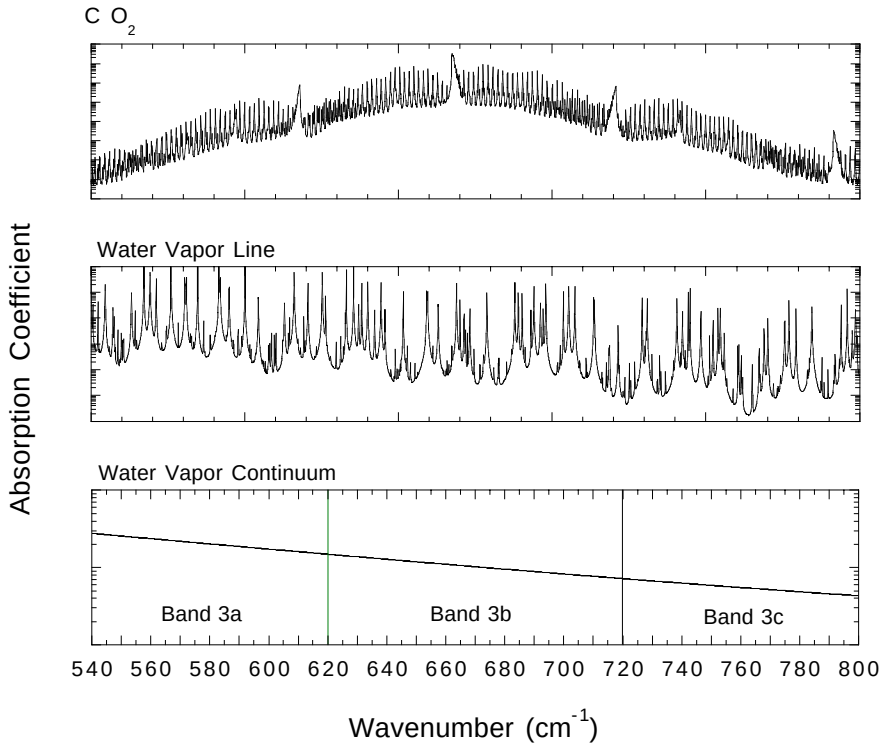

Figure 2. Schematic of the absorption coefficient for CO_2 and for water vapor line and continuum absorption in the 15-μm region (Band 3). The subdivision of the band into three sub-bands is made to accurately account for the large variations of the absorption coefficients.

The H_2O line absorption in Band 3 is computed from the *k*-distribution method. We divide the band into three sub-bands. Within each of the three sub-bands, the transmittances due to line and continuum water vapor absorption are sufficiently uncorrelated that we can overlap them using the multiplication approximation (4.27). Letting T_i^L and T_i^C be the line and continuum transmittances of sub-band *i*, we obtain the total water vapor transmittance in Band 3 by overlapping them and taking the Planck-weighted average

$$T^{WV} = \sum_{i=1}^{3} T_i^L T_i^C \left[\frac{B_i(\theta_o)}{B(\theta_o)} \right] \tag{4.28}$$

where $B_i(\theta_o)$ is the Planck flux integrated over Sub-band *i*, and $B(\theta_o)$ is the Planck flux integrated over the three sub-bands.

Substituting for the line transmittance from (4.10) and for the continuum transmittance from (4.24), we have

$$T^{WV} = \sum_{i=1}^{3} e^{-k_i{}^c w^c/\bar{\mu}} \sum_{n=1}^{N} e^{-k_n w/\bar{\mu}} (\Delta g)_{n,i} \left[\frac{B_i(\theta_o)}{B(\theta_o)} \right]$$
$$= \sum_{i=1}^{3} e^{-k_i{}^c w^c/\bar{\mu}} \sum_{n=1}^{N} e^{-k_n w/\bar{\mu}} (\Delta \hat{g})_{n,i} \qquad (4.29)$$

We use a single set of k_1, and η for the three water vapor sub-bands. See (4.12) for relating k_1 to k_n. Table 10 shows the values of these parameters. The pressure and temperature scaling parameters are shown in Table 3. Since we use the same scaling parameters for the three sub-bands, the scaled water vapor amounts, w and w^c, are independent of sub-band. Therefore, the exponentials for the water vapor line transmittance in the inner summation of (4.29) only need to be evaluated once.

Table 10. The first value of the absorption coefficient $k_1 / \bar{\mu}$ for the water vapor line absorption, the value of η that $k_n = \eta k_{n-1}$, and the Planck-weighted k-distribution function ($\Delta \hat{g}$) given by (4.29) and (4.30) of the three sub-bands in the 15 μm region.

	WATER VAPOR			CO_2	
	Subband a	Subband b	Subband c	Wings	Center
$k_1 / \bar{\mu}$	1.33e-2	1.33e-2	1.33e-2	2.66e-5	2.66e-3
η	8	8	8	8	8
$(\Delta \hat{g})_1$	.1782	.0923	.0000	.1395	.0766
$(\Delta \hat{g})_2$	.0593	.1675	.1083	.1407	.1372
$(\Delta \hat{g})_3$	.0215	.0923	.1581	.1549	.1189
$(\Delta \hat{g})_4$	.0068	.0187	.0455	.1357	.0335
$(\Delta \hat{g})_5$	.0022	.0178	.0274	.0182	.0169
$(\Delta \hat{g})_6$	.0000	.0000	.0041	.0220	.0059

The continuum absorption coefficients, k^c, are given in Table 9. Note that the coefficients for Sub-bands 3a and 3b are integer multiples of the coefficient for Sub-band 3c; thus only one

exponentiation for the water vapor continuum transmittance needs to be performed in evaluating T^{WV} for the three sub-bands.

The CO_2 transmittance may be computed either using the *k*-distribution method or using table look-up. When the table look-up is used, a single transmittance is computed directly for the entire band. When the *k*-distribution method is used, we separate Sub-band b (the center region) from Sub-bands 3a and 3c (the wings). The optical properties of Sub-bands 3a and 3c are very similar, and so we have combined them by using the same scaling parameters (p_r, θ_r, α, β, and m in Table 3 and k_1 in Table 10). The band-averaged CO_2 transmittance for Band 3 is thus computed from

$$T^{CO_2} = \sum_{n=1}^{N} e^{-(k_c)_n u_c / \bar{\mu}} (\Delta \hat{g}_c)_n + \sum_{n=1}^{N} e^{-(k_w)_n u_w / \bar{\mu}} (\Delta \hat{g}_w)_n \tag{4.30}$$

where the subscripts *c* and *w* denote, respectively, the band center (Sub-band 3b) and band wings (Sub-band 3a and 3c), and u_c and u_w are the scaled CO_2 amount in the band center and band wings. Note that

$$\sum_{n=1}^{N} (\Delta \hat{g}_c)_n + (\Delta \hat{g}_w)_n = 1 \tag{4.31}$$

Values of $(\Delta \hat{g})_n$ are given in Table 10.

Finally, the total flux transmittance in the 15-μm band is computed from

$$T = T^{WV} T^{CO_2} \tag{4.32}$$

5. SPECIAL TREATMENT OF THE 17-μm N_2O BAND

The spectral range of the absorption due to N_2O in the 17-μm region is relatively narrow (560-620 cm^{-1}) and coincides approximately with the Sub-band 3a. As shown in Figure 2, the absorption in this subband differs significantly from Sub-bands 3b and 3c. Therefore, the absorption due to N_2O in this band is treated differently from the others and is designated as Band 10 shown in Table 1. Only the changes in fluxes due to the N_2O absorption are computed. From (3.9) and (3.10), the change in fluxes can be computed from

$$\Delta F_{3a}{}^{\downarrow}(p) = \int_0^p B_{3a}(\theta') \frac{\partial[\Delta T_{3a}(p,p')]}{\partial p'} dp' \tag{5.1}$$

$$\Delta F_{3a}{}^{\uparrow}(p) \approx \varepsilon_i B_{3a}(\theta_s) \Delta T_{3a}(p,p_s) + \int_{p_s}^p B_{3a}(\theta') \frac{\partial[\Delta T_{3a}(p,p')]}{\partial p'} dp' \tag{5.2}$$

In the above equations, the change in the mean transmittance due to N_2O is defined as

$$\Delta T_{3a} = T^*{}_{3a} - T_{3a} = T^L{}_{3a} T^C{}_{3a} T^{CO_2}{}_{3a} \left[T^{N_2O}{}_{3a} - 1 \right] \tag{5.3}$$

where the subscript 3a denotes Sub-band 3a, the superscript * denotes inclusion of the N_2O absorption, and the superscripts L, C, CO_2 and N_2O denote water vapor line, water vapor continuum absorption, CO_2 and N_2O respectively. The upward and downward fluxes are then adjusted according to

$$F^{*\downarrow}(p) = F^{\downarrow}(p) + \Delta F_{3a}{}^{\downarrow}(p) \tag{5.4}$$

$$F^{*\uparrow}(p) = F^{\uparrow}(p) + \Delta F_{3a}{}^{\uparrow}(p) \tag{5.5}$$

The transmission functions are computed using the *k*-distribution method (4.10) for T^L, T^{CO_2} and T^{N_2O}, and the one-parameter scaling method (4.24) for T^C. The parameters used for computing the transmission functions of Band 10 are given in Tables 3-6.

6. CLOUDS

6.1 Cloud Single-Scattering Properties

Scattering by clouds is parameterized separately for water droplets and ice particles. The high-spectral resolution extinction coefficient, the single-scattering albedo, and the asymmetry factor were computed from the Mie theory for water droplets and the method of Fu and Sun (1998) for hexagonal ice particles. Dr. Si-Chee Tsay of NASA/Goddard Space Flight Center provided us data of these parameters for water drops, and Prof. Qiang Fu of the University of Washington provided us the data for ice particles. Mean values of the extinction coefficient β, single-scattering albedo ω, and asymmetry factor g are in turn derived for each spectral band according to

$$\beta(r_e) = \sum_{\Delta\nu} \beta_\nu(r_e) B_\nu(\theta_o) \Big/ \sum_{\Delta\nu} B_\nu(\theta_o) \tag{6.1}$$

$$\omega(r_e) = \sum_{\Delta\nu} \omega_\nu(r_e)\beta_\nu(r_e) B_\nu(\theta_o) \Big/ \sum_{\Delta\nu} \beta_\nu(r_e) B_\nu(\theta_o) \tag{6.2}$$

$$g(r_e) = \sum_{\Delta\nu} g_\nu(r_e)\omega_\nu(r_e)\beta_\nu(r_e) B_\nu(\theta_o) \Big/ \sum_{\Delta\nu} \omega_\nu(r_e)\beta_\nu(r_e) B_\nu(\theta_o) \tag{6.3}$$

where r_e is the effective radius of cloud particles, B is the Planck function, θ_o is a medium value of the atmospheric temperature set to be 250 K, and $\Delta\nu$ is the spectral interval of a band. We fit the mean single-scattering parameters by the following functions of r_e,

$$\beta(r_e) = c_{\beta,1} + \frac{c_{\beta,2}}{(r_e)^{c_{\beta,3}}} \qquad \text{for ice particles} \tag{6.4a}$$

$$= \sum_{i=1}^{4} c_{\beta,i}\, r_e^{\,i-1} \qquad \text{for liquid drops} \tag{6.4b}$$

$$\omega(r_e) = \sum_{i=1}^{4} c_{\omega,i}\, r_e^{\,i-1} \qquad \text{for both ice and liquid water particles} \tag{6.5}$$

$$g(r_e) = \sum_{i=1}^{4} c_{g,i}\, r_e^{\,i-1} \qquad \text{for both ice and liquid water particles} \tag{6.6}$$

Tables 11-13 list values of the regression coefficients, c_β, c_ω, c_g, for both water droplets and ice particles. Finally, the cloud optical thickness is derived from

$$\tau = \beta \ \text{CWP} \tag{6.7}$$

where CWP is the cloud water path (column mass per unit area), either ice or liquid water. In the current version of the code, the effective radii r_e are input parameters and are not computed within the code.

Table 11a. Coefficients for computing the extinction coefficient for cloud ice particles from (6.4a). Units of the particle size in (6.4a) are μm..

Band	$c_{\beta,1}$	$c_{\beta,2}$	$c_{\beta,3}$
1	-0.44171	0.61222	0.06465
2	-0.13727	0.54102	0.28962
3	-0.01878	1.19270	0.79080
4	-0.01896	0.78955	0.69493
5	-0.04788	0.69729	0.54492
6	-0.02265	1.13370	0.76161
7	-0.01038	1.46940	0.89045
8	-0.00450	1.66240	0.95989
9	-0.00044	2.01500	1.03750
10	-0.02956	1.06430	0.71283

Table 11b. Coefficients for computing the extinction coefficient for cloud liquid water droplets from (6.4b). Units of the particle size in (6.4b) are μm.

Band	$c_{\beta,1}$	$c_{\beta,2}$	$c_{\beta,3}$	$c_{\beta,4}$
1	0.08641	0.01769	-1.5572E-3	3.4896E-5
2	0.22027	0.00997	-1.8719E-3	5.3112E-5
3	0.38074	-0.03027	1.0154E-3	-1.1849E-5
4	0.15587	0.00371	-7.7705E-4	2.0547E-5
5	0.05518	0.04544	-4.2067E-3	1.0184E-4
6	0.12724	0.04751	-5.2037E-3	1.3711E-4
7	0.30390	0.01656	-3.5271E-3	1.0828E-4
8	0.63617	-0.06287	2.2350E-3	-2.3177E-5
9	1.15470	-0.19282	1.2084E-2	-2.5612E-4
10	0.34021	-0.02805	1.0654E-3	-1.5443E-5

Table 12a. Coefficients for computing the single-scattering albedo for cloud ice particles from (6.5). Units of the particle size in (6.5) are μm.

Band	$c_{\omega,1}$	$c_{\omega,2}$	$c_{\omega,3}$	$c_{\omega,4}$
1	0.17201	1.8814E-2	-3.5117E-4	2.1127E-6
2	0.81470	-4.1989E-3	2.3152E-7	2.0992E-7
3	0.54859	-7.4266E-4	1.2865E-5	-5.7092E-8
4	0.39218	6.4180E-3	-1.1567E-4	6.9710E-7
5	0.71773	-5.1754E-3	4.6658E-5	-1.2085E-7
6	0.77345	-8.4966E-3	1.1451E-4	-5.5170E-7
7	0.74975	-8.7083E-3	1.3367E-4	-7.1603E-7
8	0.69011	-6.9766E-3	1.1674E-4	-6.6472E-7
9	0.83963	-1.0347E-2	1.4651E-4	-7.5965E-7
10	0.64860	-4.4142E-3	6.5458E-5	-3.2655E-7

Table 12b. Coefficients for computing the single-scattering albedo for cloud liquid water droplets from (6.5). Units of the particle size in (6.5) are μm.

Band	$c_{\omega,1}$	$c_{\omega,2}$	$c_{\omega,3}$	$c_{\omega,4}$
1	-0.07857	8.0875E-2	-4.3403E-3	8.1341E-5
2	-0.01338	9.3134E-2	-6.0491E-3	1.3059E-4
3	0.03710	7.3211E-2	-4.4211E-3	9.2448E-5
4	-0.00376	9.3344E-2	-5.6561E-3	1.1387E-4
5	0.40212	7.8083E-2	-5.9583E-3	1.2883E-4
6	0.57928	5.9094E-2	-5.4425E-3	1.2725E-4
7	0.68974	4.2334E-2	-4.9469E-3	1.2863E-4
8	0.80122	9.4578E-3	-2.8508E-3	9.0078E-5
9	1.02340	-2.6204E-2	4.2552E-4	3.2160E-6
10	0.05092	7.5409E-2	-4.7305E-3	1.0121E-4

Table 13a. Coefficients for computing the asymmetry factor for cloud ice particles from (6.6). Units of the particle size in (6.6) are μm.

Band	$c_{g,1}$	$c_{g,2}$	$c_{g,3}$	$c_{g,4}$
1	0.57867	1.5592E-2	-2.6372E-4	1.5125E-6
2	0.72259	4.7922E-3	-4.7164E-5	2.0400E-7
3	0.76109	6.9922E-3	-1.0935E-4	5.9885E-7
4	0.86934	4.2268E-3	-7.4085E-5	4.3547E-7
5	0.89103	2.8482E-3	-3.9174E-5	2.0098E-7
6	0.86325	3.2935E-3	-3.9872E-5	1.8015E-7
7	0.85064	3.8505E-3	-4.9259E-5	2.3096E-7
8	0.86945	3.7869E-3	-5.6525E-5	3.0016E-7
9	0.80122	4.9086E-3	-5.8831E-5	2.6367E-7
10	0.73290	7.3898E-3	-1.0515E-4	5.4034E-7

Table 13b. Coefficients for computing the asymmetry factor for cloud liquid water droplets from (6.6). Units of the particle size in (6.6) are μm.

Band	$c_{g,1}$	$c_{g,2}$	$c_{g,3}$	$c_{g,4}$
1	-0.51930	0.20290	-1.1747E-2	2.3868E-4
2	-0.22151	0.19708	-1.2462E-2	2.6646E-4
3	0.14157	0.14705	-9.5802E-3	2.0819E-4
4	0.41590	0.10482	-6.9118E-3	1.5115E-4
5	0.55338	7.7016E-2	-5.2218E-3	1.1587E-4
6	0.61384	6.4402E-2	-4.6241E-3	1.0746E-4
7	0.67891	4.8698E-2	-3.7021E-3	9.1966E-5
8	0.78169	2.0803E-2	-1.4749E-3	3.9362E-5
9	0.93218	-3.3425E-2	2.9632E-3	-6.9362E-5
10	0.01649	0.16561	-1.0723E-2	2.3220E-4

6.2 Effective radius of cloud particles

For both water droplets and ice particles, the effective *radius* is defined as a function of the ratio of the particle volume to the surface are

$$r_e = \frac{3}{4\rho_c}\frac{C}{A_c} \tag{6.8}$$

where ρ_c is the density of cloud particles, which is 0.9167 $g\ cm^{-3}$ for ice and 1.0 $g\ cm^{-3}$ for water, and C is the cloud ice/water mass concentration per unit volume.

McFarquhar (2000) parameterized the effective size of ice particles with mixed habits (shapes) that fits the anvil clouds measured during CEPEX,

$$r_i = 0.65 \times 10^{d_0(T) + d_1(T)z + d_2(T)z^2 + d_3(T)z^3} \tag{6.9}$$

where $z = log_{10}(C)$. Tables for the regression coefficients *d's* are given in McFarquhar (2000). The effective particle *diameter* in the McFarquhar's parameterization is defined as

$$D_e = \frac{2\sqrt{3}}{3\rho_c}\frac{C}{A_c} \tag{6.10}$$

The constant 0.65 in (6.9) is a factor that converts the effective *diameter* defined by Equation (6.10) to the effective *radius* defined by Equation (6.8). (r_i = 0.65 D_e). Units are $g\ m^{-3}$ for C and μm for r_i.

Szczodrak et al. (2001) retrieved the cloud optical thickness and the effective mean particle size using the AVHRR radiance measurements of marine boundary-layer water clouds in the eastern Pacific and the ocean near Tasmania. They found that the effective radius (μm) of water droplets is related to the optical thickness in the visible spectral region by

$$r_w \propto \tau_c^{1/5}$$

From the results shown in their Figs. 4, 6, and 11, we have made the following approximation,

$$r_w = 5.8\tau_c^{1/5} \tag{6.11}$$

From Equations (6.7) and (6.11) and the relation between τ_c and r_w, we then have

$$r_w = 4.7CWP^{0.1667} \tag{6.12}$$

where *CWP* is cloud water path in $g\ m^{-2}$.

The *CWP* in (6.12) refers to the liquid water amount of the entire cloud layer, However, the value of *CWP* of an atmospheric layer depends upon the thickness of the layer, which varies from model to model. When Equation (6.12) is applied to a model layer, the cloud particle size would depend on the thickness of a model layer. This is, of course, physically incorrect.

Therefore, Equation (6.12) cannot be appropriately applied a model layer, where *CWP* and, hence, r_w depend on the layer thickness.

For the thickness of a boundary-layer cloud Δz_c, Equation (6.12) can be reduced to

$$r_w = 4.7\left(C\Delta z_c\right)^{0.1667} = 14.3C^{0.1667} \tag{6.13}$$

where C is the cloud water concentration in $g\ m^{-3}$, and Δz_c is assumed to be 800 meters. Since C is not a function of the thickness of a model layer, the use of (6.13) does not have the problem of using (6.12). It can be seen from (6.13) that r_w is not very sensitive to Δz_c. An uncertainty of 50% in Δz_c induces only an uncertainty of 7% in r_w.

6.3 Layer optical properties

When the absorption and scattering due to clouds interact with that of gases and aerosols in a layer, the effective optical thickness, single-scattering albedo, and asymmetry factor in a spectral band are computed from

$$\tau = \sum_i \tau_i \tag{6.14}$$

$$\overline{\omega} = \sum_i \omega_i \tau_i \Big/ \sum_i \tau_i \tag{6.15}$$

$$\overline{g} = \sum_i g_i \omega_i \tau_i \Big/ \sum_i \omega_i \tau_i \tag{6.16}$$

where the summation is over all gases, aerosols, and liquid water and ice particles, *i*. Thus, in the *LW* radiation code, ice and liquid water cloud particles are allowed to mix in a layer.

6.4 Paramaterization for Cloud Scattering

Explicit calculations of scattering by clouds requires a large amount of computer time. Instead, we scale the cloud optical thickness τ to approximate the effect of scattering according to

$$\tau^c = (1 - \omega f)\tau \tag{6.17}$$

where f is the fraction of radiation scattered downward (upward) for radiation incident from above (below). This scaling takes into account the effect of back-scattering and absorption by cloud particles.

Assuming that the scattering phase function can be approximated by the Henyen-Greenstein function, the forward-scattering function f is computed as a function of the asymmetry factor and fit by a polynomial function

$$f = \sum_{i=1}^{4} a_i g^{i-1} \tag{6.18}$$

where $a_1 = 0.5$, $a_2 = 0.3738$, $a_3 = 0.0076$, and $a_4 = 0.1186$.

Thus, the cloud optical thickness is reduced from τ to τ^c, and scattering is not explicitly computed. By scaling the cloud optical thickness (6.17), the effect of scattering is parameterized but not explicitly computed. The computing time is the same as the case without taking into account the cloud scattering. See Chou et al. (1999) for details of the parameterization for the cloud *LW* scattering.

6.5 Cloud Overlapping

Equation (2.3) applies to the case where the atmosphere is horizontally homogeneous. When clouds with fractional areal cover occur at different heights, assumptions have to be made on the ways these clouds are overlapped for radiative flux calculations. There are a number of schemes used to vertically associate clouds at different height (e. g. Manabe and Strickler, 1964; Geleyn and Hollingsworth, 1979; Liang and Wang, 1997; Raisanen 1998; Li., 2000). These schemes all assume that clouds either are randomly overlapped or have a combination of random and maximum overlapping. In our radiation parameterization, we also adopt a maximum-random overlapping cloud scheme.

If a cloud layer with fractional cover A and optical thickness τ_v^c is introduced between p and p', the mean radiance transmittance in the direction μ becomes

$$[1-A]e^{-\tau_v(p,p')/\mu} + Ae^{-\left[\tau_v(p,p')+\tau_v{}^c(p,p')\right]/\mu}$$

and the mean flux transmittance is

$$\begin{aligned} T_v{}^*(p,p') &= 2\int_0^1 \left\{ [1-A]e^{-\tau_v(p,p')/\mu} + Ae^{-\left[\tau_v(p,p')+\tau_v{}^c\right]/\mu} \right\} \mu d\mu \\ &= \left[1 - A(1-e^{-\tau_v{}^c/\bar{\mu}})\right] T_v(p,p') \end{aligned} \tag{6.19}$$

where τ_v is the optical thickness of a clear atmosphere, $\bar{\mu}$ is the effective mean value of μ which converts the radiance transmittance to flux transmittance, and T_v is the transmittance of a clear atmosphere defined by (2.3). The diffusivity factor $1/\bar{\mu}$ depends on τ_v but is commonly chosen to be 1.66. Letting $N_v = A(1-e^{-\tau_v{}^c/\bar{\mu}})$, Equation (6.19) becomes

$$T_v{}^*(p,p') = (1-N_v)T_v(p,p') \tag{6.20}$$

If we further assume that τ_v^c is constant within a spectral band and integrate Equation (6.20) over the band, we have

$$T^*(p,p') = (1-N)T(p,p') \tag{6.21}$$

where *T* is the band-averaged flux transmittance defined by (3.7). Because $1-e^{-\tau^c/\bar{\mu}}$ is the flux emissivity of the cloud layer, *N* can be regarded as the effective cloud cover with an emissivity of 1. Alternatively, *(1-N)* can be regarded as the effective cloud transmissivity with a fractional cloud cover of 1.

When there is more than one cloud layer with fractional cover between *p* and *p'*, the situation is considerably more complicated since we need to describe how the clouds are overlapped. In general we can write

$$T^*(p,p') = C(p,p')T(p,p') \tag{6.22}$$

where *C(p,p')* depends on the values of *A* and τ^c for the various cloud layers.

For the special case of any combination of overcast and *randomly overlapped* fractional cloud layers, we have

$$C(p,p') = \prod_j (1-N_j) \tag{6.23}$$

where the subscript *j* denotes the cloud layers between *p* and *p'*. Since $\prod(1-N_j)$ is the fraction of the horizontal area that would be cloud-free if all cloud layers (including overcast layers) were assigned their equivalent black-cloud fraction and then randomly overlapped, Harshvardhan et al. (1987) referred to *C(p,p')* as the probability of a clear line-of-sight between *p* and *p'*. Obtaining *C(p,p')* for non-random arrangements of gray clouds, however, is not as straightforward. In general, *C(p,p')* does not depends on *N* alone, but on more complicated combinations of *A* and τ^c.

Consider another arrangement discussed by Harshvardhan et al. (1987), that of *maximally overlapped* clouds. If the largest cloud between *p* and *p'* is black, then *C(p,p')* is simply equal to one minus its fraction. If all clouds are allowed to be gray, however, *C(p,p')* will depend on all

cloud fractions and optical thicknesses. For the maximally overlapped clouds between p and p', the clear line-of-sight $C(p,p')$ is independent of the order of cloud layers and may be computed by putting the clouds in order of increasing cloud cover:

For the special case with three maximally overlapped clouds between p and p', the clear line-of-sight $C(p,p')$ may be computed by putting the clouds in order of increasing cloud cover:

$$\begin{aligned} 1-C &= A_1\left[1-e^{-(\tau^c{}_1+\tau^c{}_2+\tau^c{}_3)}\right]+(A_2-A_1)\left[1-e^{-(\tau^c{}_2+\tau^c{}_3)}\right]+(A_3-A_2)\left[1-e^{-\tau^c{}_3}\right] \\ &= A_3(1-e^{-\tau^c{}_3})+\left[A_2(1-e^{-\tau^c{}_2})+A_1(1-e^{-\tau^c{}_1})e^{-\tau^c{}_2}\right]e^{-\tau^c{}_3} \\ &= N_3+\left[N_2+N_1e^{-\tau^c{}_2}\right]e^{-\tau^c{}_3} \end{aligned} \tag{6.24}$$

where $A_{j-1}<A_j$. In (6.24), we have dropped $\bar{\mu}$ from $\tau^{c/\bar{\mu}}$ for simplicity. As referenced to the upper cloud group in Figure 3, the first and second brackets represent the absorption of the regions where there are three and two cloud layers overlap, while the third bracket represents only the absorption of the largest cloud cover.

It follows from (6.24) that for the case with J maximally overlapped clouds, $C(p,p')$ may be computed by evaluating the following recursion:

$$D^{(0)} = 0 \tag{6.25}$$

$$D^{(j)} = N_j + D^{(j-1)}e^{-\tau^c{}_j/\bar{\mu}}, \qquad j = 1, \ldots, J \tag{6.26}$$

and

$$C(p,p') = 1-D^{(J)} \tag{6.27}$$

Whenever a black cloud ($\tau^c_j \to \infty$) occurs in (6.26), all smaller clouds are eliminated from the recursion. This treatment of cloud overlapping was first proposed by Chou and Suarez (1994). A similar cloud overlapping scheme is also proposed by Raisanen (1998).

To provide an example for the overlapping scheme, we show in Figure 3 two groups of maximally overlapped clouds between p and p'. The upper group and the lower group are labeled U and L, respectively. These two groups are assumed randomly overlapped. The clear line-of-sight between p and p' is

$$C(p,p') = C^U C^L \tag{6.28}$$

where C^U and C^L are the clear line-of-sight of the upper and lower cloud groups computed from (6.27). Fluxes can then be computed from (3.9) and (3.10) with $T(p,p')$ replaced by $C(p,p')T(p,p')$.

In the current version of our radiation code, clouds are grouped into three height ranges: high, middle and low separated approximately by 400 *hPa* and 700 *hPa* pressure levels. Clouds within each height group are assumed maximally overlapped, and clouds among the three height groups are assumed randomly overlapped. This cloud overlapping scheme can be easily extended to include a more flexible situation that assumes maximum overlapping of adjacent cloud layers and random overlapping of cloud layers separated by clear layers, as originally proposed by Gelygn and Hollingswoth (1979).

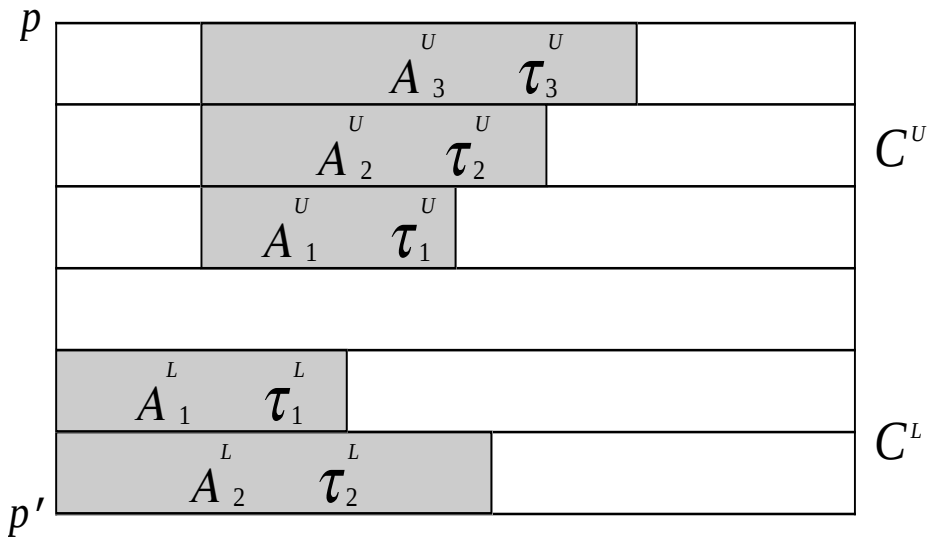

Figure 3. Schematic showing two groups of randomly overlapped clouds. Cloud layers within each group are assumed maximally overlapped. C^U and C^L are the clear line-of-sight of the upper group and lower group, respectively. The clear line-of-sight between the levels p and p' is $C^U C^L$ as shown in (6.21).

7. AEROSOLS

The aerosol optical thickness, single-scattering albedo, and asymmetry factor for each of the 10 bands and each of the atmospheric layers are specified input parameters. Different types of aerosols are allowed to co-exist in a layer. The effective optical thickness, single-scattering abledo, and asymmetry factor of a layer are computed similarly to that of clouds,

$$\tau^a = \sum_i \tau^a{}_i \tag{7.1}$$

$$\bar{\omega}^a = \sum_i \omega^a{}_i \tau^a{}_i \Big/ \sum_i \tau^a{}_i \tag{7.2}$$

$$\bar{g}^a = \sum_i g^a{}_i \omega^a{}_i \tau^a{}_i \Big/ \sum_i \omega^a{}_i \tau^a{}_i \tag{7.3}$$

where *i* is the index for aerosol type. The same parameterization for cloud scattering, (6.11) and (6.12), is applied to an aerosol-laden layer. We further assume that the aerosol layer is plane-parallel and the flux transmission function of the layer is computed from

$$T^a = T e^{-\tau^{*a}/\bar{\mu}} \tag{7.4}$$

where τ^{*a} is the scaled aerosol optical thickness according to (6.11) and (6.12), and T^a and T are flux transmittances with and without aerosols.

8. VERTICAL DISCRETIZATION

8.1 Downward and Upward Fluxes

To approximate the vertical integrals in (3.9) and (3.10), the atmosphere is divided into *L* layers numbered as shown in Figure 4. The downward and upward fluxes at level *l* for the *ith* band are computed from

$$F_{i,l}{}^{\downarrow} = \sum_{l'=1}^{l-1} B_{i,l'+\frac{1}{2}} \left[T_i(l,l'+1) - T_i(l,l') \right] \qquad l = 2, ..., L+1 \tag{8.1}$$

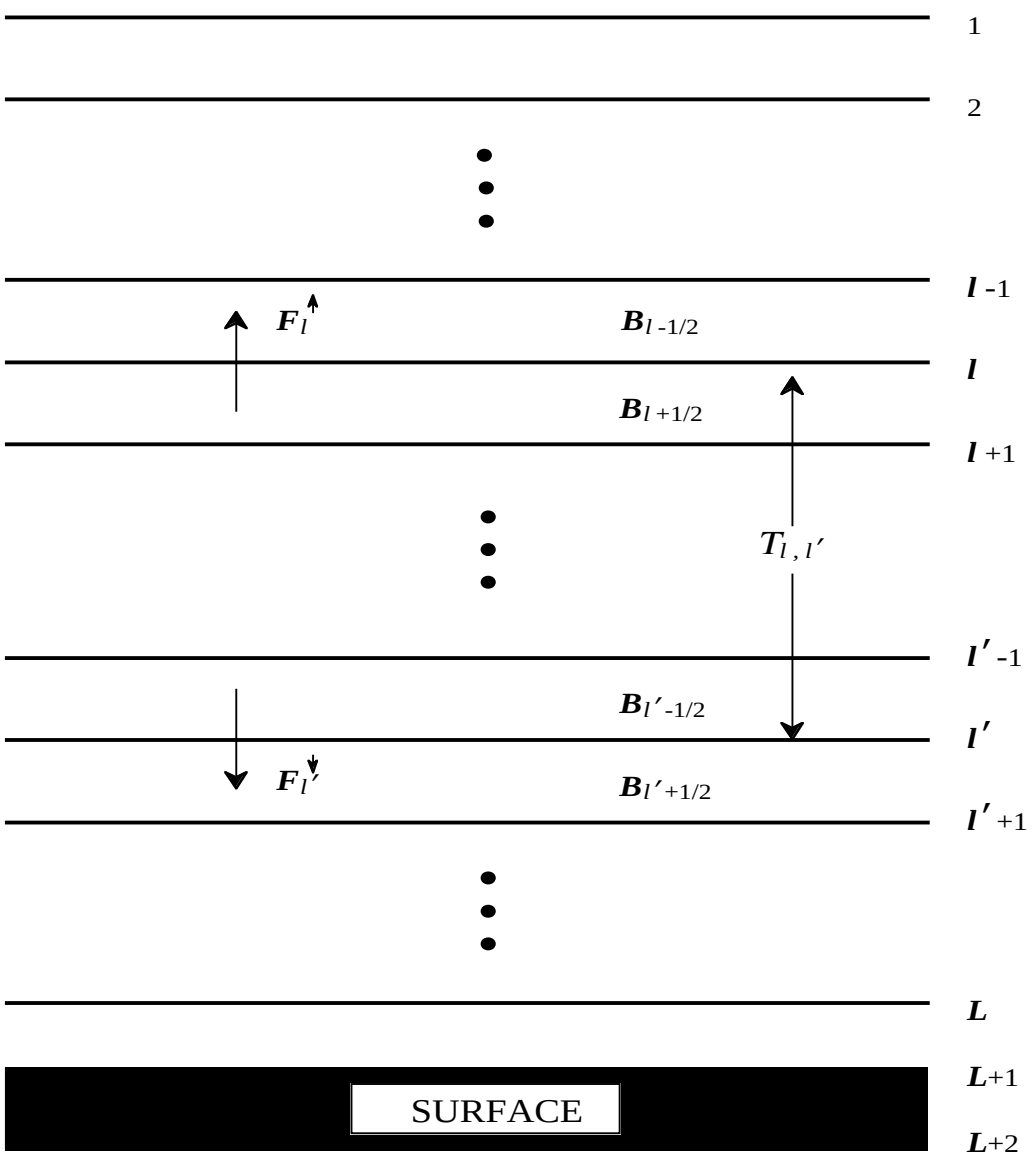

Figure 4. The vertical grid and placement of various quantities for an atmosphere consisting of L layers. Quantities defined at the layers, such as the Planck flux, B are denoted by half-integer subscripts, and quantities defined at the levels separating layers, such as the downward and upward fluxes F, by integer subscripts. The transmittance shown is for a multi-layer region bounded by levels l and l'. Note that the surface is treated as a fictitious layer at $L+3/2$.

$$F_{i,l}^{\uparrow} = \sum_{l'=l}^{L} B_{i,l'+\frac{1}{2}} \left[T_i(l,l') - T_i(l,l'+1) \right] + T_i(l,L+1) F_{i,L+1}^{\uparrow} \qquad l = 1, ..., L \qquad (8.2)$$

$$F_{i,1}^{\downarrow} = 0 \qquad (8.3)$$

$$F_{i,L+1}^{\uparrow} = \varepsilon_i B_i(\theta_s) + (1-\varepsilon_i) F_{i,L+1}^{\downarrow} \qquad (8.4)$$

where $B_{i,l+1/2}$ is the Planck flux at the temperature $\theta_{l+1/2}$ integrated over the band i, $T_i(l,l')$ is the Planck-weighted flux transmittance between the levels l and l', $T_i(l,L+1)$ is the transmittance between the level l and the Earth's surface, and θ_s is the Earth's surface temperature.

By rearranging terms in Equations (8.1) and (8.2) and defining

$$\Delta F_i^{\downarrow}(l,l') = T_i(l,l') \left(B_{i,l-\frac{1}{2}} - B_{i,l+\frac{1}{2}} \right) \qquad l' > l, \quad l=1, 2, \ldots, L \qquad (8.5)$$

$$\Delta F_i^{\uparrow}(l,l') = T_i(l,l') \left(B_{i,l'-\frac{1}{2}} - B_{i,l'+\frac{1}{2}} \right) \qquad l' > l, \quad l=1, 2, \ldots, L \qquad (8.6)$$

$$B_{i,\frac{1}{2}} = 0 \qquad (8.7)$$

$$B_{i,L+\frac{3}{2}} = \varepsilon_s B_i(\theta_s) \qquad (8.8)$$

the downward and upward fluxes can be written as

$$F_{i,l'}^{\downarrow} = B_{i,l'-\frac{1}{2}} + \sum_{l=1}^{l'-1} \Delta F_i^{\downarrow}(l,l') \qquad l'=2, 3, \ldots, L+1 \qquad (8.9)$$

$$F_{i,l}^{\uparrow} = B_{i,l+\frac{1}{2}} + T_i(l,L+1)(1-\varepsilon_i) F_{i,L+1}^{\downarrow} - \sum_{l'=l+1}^{L+1} \Delta F_i^{\uparrow}(l,l') \qquad l =1, 2, \ldots, L \qquad (8.10)$$

As opposed to (8.1) and (8.2), only one transmittance, $T_i(l,l')$, appears in each term under the summation in (8.9) and (8.10). The sums can be build-up term by term. When the

transmittance of a layer bounded by the upper level l and the lower level l' is computed, the downward flux at l' and upward flux at l are immediately updated. In this way, there is no need to store the transmittance matrix. The storage of the entire routine scales then like L, rather than L^2 – a very significant advantage for models with high vertical resolution.

8.2 Emission of a Layer

When a layer is rather opaque and the temperature range across the layer is large, the difference between the upward and downward emission of the layer will also be large. For the case of an optically thick cloud layer, the upward emission will be at the temperature of the cloud-top, and the downward emission will be at the temperature of the cloud base. The use of the emission at the layer-mean temperature, as shown in (8.1) and (8.2), will overestimates the outgoing longwave radiation at the top of the atmosphere and enhance the cooling (or reduce the heating) of the cloud layer. Generally, the effective emitting temperature of a rather opaque layer is close to the temperature at the top of the layer for upward emission and close to the bottom temperature of the layer for downward emission. Therefore, it is desirable to compute separately the upward emission and downward emission of a layer.

The contribution to the upward flux at the level p from the layer *below* can be written as

$$\begin{aligned} \Delta F^{\uparrow}(p) &= -\int_{p}^{p+\Delta p} B(p')\left[\partial T(p,p')/\partial p'\right]dp' \\ &= B^{u}(1-T_o) \end{aligned} \tag{8.11}$$

where Δp is the thickness of the layer, B^u is the effective Planck flux of the layer, and $T_o = T(p + \Delta p, p)$ is the flux transmittance between p and $p + \Delta p$.

The Planck flux $B(p')$ varies slowly within a layer, but the transmittance $T(p, p')$ decreases exponentially as p' departs from p. For $T_o \to 0$, the layer is rather opaque, and the radiation primarily comes from regions close to the level p. The effective Planck flux B^u for this case should be close to $B(p)$. On the other hand, if the layer is rather transparent ($T_o \to 1$), the transmitttance varies slowly with p' and the flux at p is contributed more or less evenly from the entire layer. By linearizing the Plank flux within the layer, it follows that $B^u \to B(p + \Delta p/2)$ for $T_o \to 1$. Calculations of the flux contribution from the layer should take into account the dependence of B^u on T_o.

Assuming that the Planck function varies linearly with pressure and the Planck-weighted transmittance decreases exponentially with pressure away form *p*, we have *B(p')* = *B(p)* + *[B(p+Δp) - B(p)] (p'-p) / Δp* and $T(p,p') = e^{-c(p'-p)}$, where c is a constant. It follows from (8.11) that the effective Planck flux of the layer is

$$B^u = \left[\frac{B(p) - B(p+\Delta p)T_o}{1-T_o}\right] + \left[\frac{B(p) - B(p+\Delta p)}{\ln T_o}\right] \tag{8.12}$$

Equation (8.12) meets the conditions that $B^u \to B(p)$ for $T_o \to 0$, and $B^u \approx \left[B(p+\Delta p) + B(p)\right]/2$ for weak absorption when $T_o \approx 1 - c\Delta p + \frac{1}{2}(c\Delta p)^2$.

Similarly, for the downward flux at the lower boundary of the layer, the effective Planck function of the layer is

$$B^d = \left[\frac{B(p+\Delta p) - B(p)T_o}{1-T_o}\right] + \left[\frac{B(p+\Delta p) - B(p)}{\ln T_o}\right] \tag{8.13}$$

From (8.12) and (8.13), we have

$$B^d + B^u = B(p) + B(p+\Delta p) \tag{8.14}$$

By replacing $B_{i,l'-0.5}$ and $B_{i,l+0.5}$ with B^d and B^u, Equations (8.9) and (8.10) reduce to

$$F_{i,l'}{}^{\downarrow} = B^d{}_{i,l'-\frac{1}{2}} + \sum_{l=1}^{l'-1} T_i(l,l')\left(B^d{}_{i,l-\frac{1}{2}} - B^d{}_{i,l+\frac{1}{2}}\right) \tag{8.15}$$

$$F_{i,l}{}^{\uparrow} = B^u{}_{i,l+\frac{1}{2}} + T_i(l,L+1)(1-\varepsilon_s)F_{i,L+1}{}^{\downarrow} - \sum_{l'=l+1}^{L+1} T_i(l,l')\left(B^u{}_{i,l'-\frac{1}{2}} - B^u{}_{i,l'+\frac{1}{2}}\right) \tag{8.16}$$

where

$$B^d{}_{i,l'-\frac{1}{2}} = \left[\frac{B_{i,l'} - B_{i,l'-1}T_i(l',l'-1)}{1-T_i(l',l'-1)}\right] + \left[\frac{B_{i,l'} - B_{i,l'-1}}{\ln T_i(l',l'-1)}\right] \tag{8.17}$$

$$B^u{}_{i,l'-\frac{1}{2}} = \left(B_{i,l'} + B_{i,l'-1}\right) - B^d{}_{i,l'-\frac{1}{2}} \tag{8.18}$$

For a layer partially filled with clouds, the mean transmission is approximated by

$$T_i = (1-A)T_i^{clr} + AT_i^{clr}T_i^{cld} \tag{8.19}$$

where A is the fractional cloud cover, and *clr* and *cld* denote clear and cloudy. When a model layer spans a region where the temperature lapse rate changes signs, we cannot assume that B linearly varies with p, and Equations (8.17) and (8.18) are no longer valid. In such a case, we simply compute B^d and B^u from

$$B^u_{\,i,l+\frac{1}{2}} = B^d_{\,i,l'-\frac{1}{2}} = 0.5B_{\,i,l+\frac{1}{2}} + 0.25\left(B_{i,l} + B_{i,l'}\right) \tag{8.20}$$

8.3 The k-Distribution Transmission Functions

For gaseous absorption using the k-distribution method, the transmittance of each of the k-intervals can be first computed for the L layers from

$$\Delta T_{\,n,l+\frac{1}{2}} = e^{-k_n \Delta w_{l+1/2}/\overline{\mu}} \qquad l = 1, 2. \ldots, L; \quad n = 1, 2, \ldots, N \tag{8.21}$$

where k_n is the absorption coefficient of the n^{th} k-interval, and $\Delta w_{l+1/2}$ is the *scaled* absorber amount of the layer between the levels l and l+1. Both k and Δw vary with the spectral interval i. *This index is dropped for simplicity*. Because the set of *k's* are chosen according to (4.12), we need only to compute the exponential for the first value of k, and the others can be derived from

$$\Delta T_n = \left(\Delta T_{n-1}\right)^{\eta} \qquad n = 2, 3, \ldots, N \tag{8.22}$$

Once ΔT_1 is computed, the computation of each of the ΔT_n with n>1 requires only a few multiplication operations.

The transmittance between an upper level l and an lower level l', i.e. $l' > l$, is given by

$$T_n(l,l') = \prod_{j=l}^{l'-1} \Delta T_{\,n,j+\frac{1}{2}} \qquad l = 1, \ldots, \; L; \; l' = l+1, \ldots, L+1 \tag{8.23}$$

and the transmittance between the level l and the surface is given by

$$T_n(l,L+1) = \prod_{j=l}^{L} \Delta T_{\,n,j+\frac{1}{2}} \tag{8.24}$$

Following (4.10), the band-averaged transmission terms in (8.5) and (8.6) are computed from

$$T(l,l') = \sum_{n=1}^{N} T_n(l,l')\Delta g_n \tag{8.25}$$

8.4 Table Look-Up for Transmission Functions

When using the pre-computed transmittance tables, the transmittance between the upper level l and the lower level l' is derived from

$$T_{l,l'} = T(u_{l,l'}, \bar{p}_{l,l'}, \bar{\theta}_{l,l'}) \tag{8.26}$$

where u is the (non-scaled) absorber amount, and $\bar{p}$ and $\bar{\theta}$ are the effective pressure and temperature. They are defined by

$$u_{l,l'} = \sum_{j=l}^{l'-1} \Delta u_{j+\frac{1}{2}} \tag{8.27}$$

$$\bar{p}_{l,l'} = \frac{\sum_{j=l}^{l'-1} p_{j+\frac{1}{2}} \Delta u_{j+\frac{1}{2}}}{\sum_{j=l}^{l'-1} \Delta u_{j+\frac{1}{2}}} \tag{8.28}$$

$$\bar{\theta}_{l,l'} = \frac{\sum_{j=l}^{l'-1} \theta_{j+\frac{1}{2}} \Delta u_{j+\frac{1}{2}}}{\sum_{j=l}^{l'-1} \Delta u_{j+\frac{1}{2}}} \tag{8.29}$$

where $j+1/2$ denotes the layer between the levels j and $j+1$. Equations (8.28) - (8.29) follow Eqs. (4.13) - (4.14). In (8.26), the transmittance T varies with the spectral band i. *This index is dropped for simplicity.*

9. SUB-GRID VARIATIONS OF LAND SURFACE

If the size of a model grid-box is greater than tens of kilometers, the variations of surface temperature and emissivity within the grid box could have a significant effect on model simulations. In such a case, the emissivity and reflectivity of the model surface should include the

effect of the sub-grid variations. Let us consider a vegetation-covered land surface characterized by a ground-skin temperature θ_g, vegetation canopy temperature θ_v, ground emissivity ε_g, canopy emissivity ε_v, and canopy reflectivity r_v. The radiation emitted by the ground and the vegetation that leaves the top of the canopy is given by

$$E = \frac{T_v\left[\varepsilon_g B(\theta_g) + r_g \varepsilon_v B(\theta_v)\right]}{(1 - r_v r_g)} + \varepsilon_v B(\theta_v) \tag{9.1}$$

where $r_g = (1\text{-}\varepsilon_g)$ is the ground reflectivity, and $T_v = (1\text{-}\varepsilon_v\text{-}r_v)$ is the canopy transmissivity. The first term within the bracket is the radiation emitted by the ground, the second term within the bracket is the radiation emitted downward by the vegetation and subsequently reflected by the ground, and the last term is the upward emission by the vegetation. The denominator in (9.1) takes care of the multiple reflections between the vegetation and the ground.

The downward flux from the atmosphere is reflected by the vegetation and the ground. This term is given by

$$R = rF^{\downarrow}(p_s) \tag{9.2}$$

where r is the effective reflectivity of the canopy and the ground given by

$$r = r_v + \frac{r_g T_v^{\,2}}{(1 - r_v r_g)} \tag{9.3}$$

For the case without vegetation cover, we have $T_v = 1$, $\varepsilon_v = r_v = 0$, and Equations (9.1) and (9.3) reduce to

$$E = \varepsilon_g B(\theta_g) \tag{9.4}$$

$$r = r_g \tag{9.5}$$

It should be noted that Equations (3.10), (8.2) and (8.4) are derived based on (9.4) and (9.5).

If there are N sub-grid boxes in a model box with fractional cover f_n, $n = 1, 2, \ldots N$, Equations (9.1) and (9.3) become

$$E = \sum_{n=1}^{N} f_n \left\{ \frac{T_{v,n}\left[\varepsilon_{g,n} B(\theta_{g,n}) + r_{g,n}\varepsilon_{v,n} B(\theta_{v,n})\right]}{(1 - r_{v,n} r_{g,n})} + \varepsilon_{v,n} B(\theta_{v,n}) \right\} \tag{9.6}$$

$$r = \sum_{n=1}^{N} f_n \left[r_{v,n} + \frac{r_{g,n} {T_{v,n}}^2}{(1 - r_{v,n} r_{g,n})} \right] \tag{9.7}$$

where

$$\sum_{n=1}^{N} f_n = 1 \tag{9.8}$$

and the subscript n denotes the sub-grid box.

For the case without vegetation cover, Equations (9.6) and (9.7) reduce to

$$E = \sum_{n=1}^{N} f_n \varepsilon_{g,n} B(\theta_{g,n}) \tag{9.9}$$

$$r = \sum_{n=1}^{N} f_n r_{g,n} \tag{9.10}$$

With E and r given above and R given by (9.2), Equations (8.2) and (8.4) reduce to the following general forms

$$F_l^{\uparrow} = \sum_{l'=l}^{L} B_{l'+\frac{1}{2}} \left[T(l,l') - T(l,l'+1)\right] + T(l,L+1) {F_{L+1}}^{\uparrow} \tag{9.11}$$

$${F_{L+1}}^{\uparrow} = E + R = E + r {F_{L+1}}^{\downarrow} \tag{9.12}$$

Finally, the partial derivative of the upward flux with respect to the surface temperature given by (3.12) reduces to the following general forms

$$E' = \sum_{n=1}^{N} f_n \left\{ \frac{T_{v,n}\left[\varepsilon_{g,n} B'(\theta_{g,n}) + r_{g,n}\varepsilon_{v,n} B'(\theta_{v,n})\right]}{(1 - r_{v,n} r_{g,n})} + \varepsilon_{v,n} B'(\theta_{v,n}) \right\} \tag{9.13}$$

$$\frac{\partial F^{\uparrow}(p)}{\partial \theta_s} = T(p, p_s)E' \tag{9.14}$$

where $B'(\theta)$ is the derivative of B with respect to temperature at θ. For simplicity, we have omitted the index for the spectral band i in all of the equations.

10. COMPARISONS WITH LINE-BY-LINE CALCULATIONS

Fluxes and cooling rate computed using the transmittance parameterizations are compared with high spectral-resolution *line-by-line* calculations. Our *line-by-line* calculations of the absorption coefficient use the *Air Force Geophysical Laboratory 1996* edition of the molecular absorption parameters (Rothman et al., 1998). The molecular line shape is assumed to follow the Voigt function. The absorption coefficient at wavenumbers > 10 cm^{-1} from the line center is taken to be zero, which is equivalent to a line-cutoff of 10 cm^{-1}. The absorption coefficient is computed at spectral intervals of 0.001 cm^{-1} for Band 3 and 0.002 cm^{-1} for the other bands.

The mid-latitude summer atmosphere and the sub-arctic winter atmosphere taken from McClatchey et al. (1972) are used in the flux calculations. No clouds and aerosols are included. The CO_2 concentration is fixed at 350 *ppmv*, and the specific humidity above the tropopause is set to 4×10^{-6} *g/g*. The atmosphere is divided into 75 layers with $\Delta p \sim 25$ *hPa* at pressures > 100 *hPa* and $\Delta \log_{10} p = 0.15$ at pressures < 100 *hPa*.

Cooling rates computed using the *line-by-line* method (solid lines) and the parameterization with the HIGH option (dashed lines) are shown in Figures 5 and 6. The cooling rate is presented as a function of $\log_{10} p$ in the upper panels and p in the lower panels. It is noted that for the HIGH option, the transmission functions of CO_2 in Band 3 and of water vapor in Bands 1, 2, and 8 are computed using table look-up (see Table 1). It can be seen in the figures that, compared to the *line-by-line* method, the cooling rate is computed accurately. The maximum error in the stratosphere is < 0.25 $^{\circ}C/day$ and is < 0.15 $^{\circ}C/day$ in the troposphere. These errors are small when compared with the maximum cooling of ~12 $^{\circ}C/day$ in the stratosphere and ~2$^{\circ}C/day$ in the troposphere.

The downward flux at the surface and the upward flux at the top of the atmosphere are shown in Tables 14 and 15 for the mid-latitude summer atmosphere and the sub-arctic winter atmosphere, respectively. Errors are generally smaller than 1 Wm^{-2} in individual bands. Integrated over the *LW* spectrum, the parameterizations can compute the fluxes to within 1% of

the *line-by-line* calculations for the mid-latitude summer atmosphere and within 0.5% for the sub-arctic winter atmosphere.

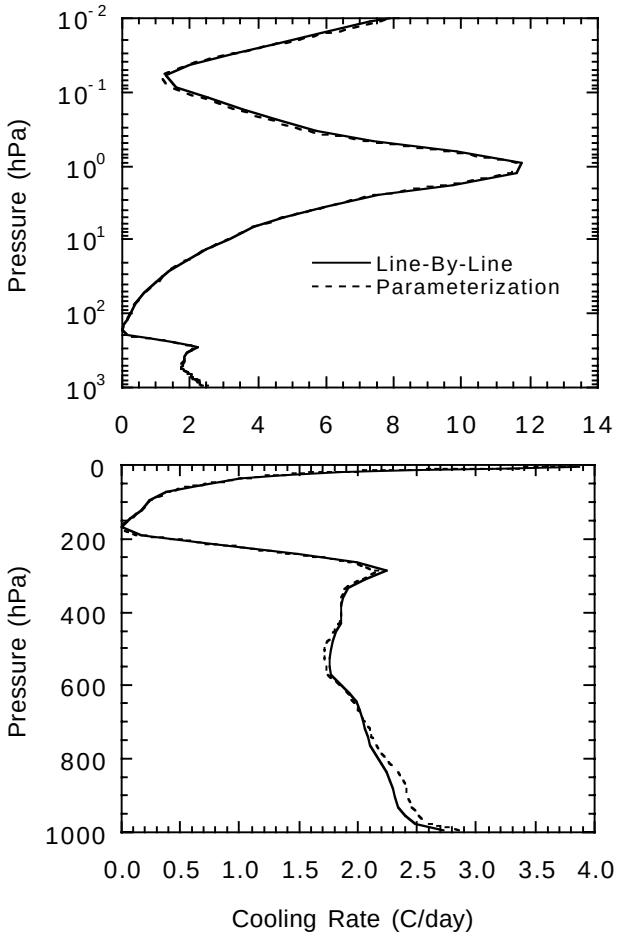

Figure 5. The cooling rate computed for a clear mid-latitude summer atmosphere using the line-by-line method (solid curves) and the "HIGH" option of the parameterization (dashed curves). Cooling is due to water vapor molecular line and continuum absorption, as well as CO_2 and O_3 absorption.

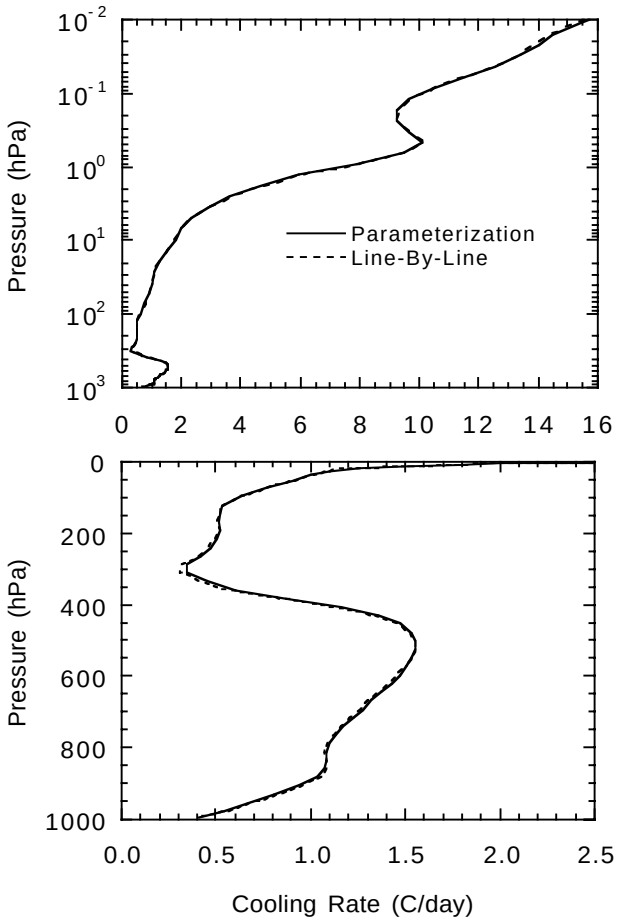

Figure 6. Same as Figure 5 except for a clear sub-arctic winter atmosphere.

Table 14. Downward fluxes at the surface, $F^{\downarrow}_{sfc}$, and upward fluxes at the top, $F^{\uparrow}_{top}$, for a clear mid-latitude summer atmosphere computed using a line-by-line method and the parameterization with the HIGH option. Units of the fluxes are Wm^{-2}.

Spectral Band (cm^{-1})	$F^{\downarrow}_{sfc}$	$F^{\uparrow}_{top}$	Absorber
0- 340			
line-by-line	51.02	34.56	H_2O (*line*)
Parameterization	51.04	34.40	H_2O (*line*)
340- 540			
line-by-line	80.76	61.01	H_2O (*line*)
Parameterization	81.23	60.54	H_2O (*line*)
540- 800			
line-by-line	105.85	67.90	H_2O (*line*, *continuum*), CO_2
Parameterization	107.29	68.29	H_2O (*line*, *continuum*), CO_2
800- 980			
line-by-line	26.89	58.62	H_2O (*line*, *continuum*), O_3
Parameterization	27.01	58.72	H_2O (*line*, *continuum*)
980-1100			
line-by-line	12.36	22.36	H_2O (*line*, *continuum*), O_3
Parameterization*	12.54	21.41	H_2O (*line*, *continuum*), O_3
1100-1215			
line-by-line	9.73	20.96	H_2O (*line*, continuum), O_3
Parameterization	9.63	21.42	H_2O (*line*, *continuum*)
1215-1380			
line-by-line	19.43	15.89	H_2O (*line*, *continuum*)
Parameterization	19.78	15.67	H_2O (*line*, *continuum*)
1380-1900			
line-by-line	30.51	7.56	H_2O (*line*)
Parameterization	30.68	7.61	H_2O (*line*)
1900-3000			
line-by-line	3.04	5.13	H_2O (*line*)
Parameterization	3.17	5.00	H_2O (*line*)
Total			
line-by-line	339.59	293.99	
Parameterization	342.37	293.03	

* The absorption due to O_3 in Bands 4 and 6 are folded into the O_3 absorption tables of this band , see Equation (4.18).

Table 15. Same as Table 14, except for a clear sub-arctic winter atmosphere.

Spectral Band (cm^{-1})	$F^{\downarrow}_{sfc}$	$F^{\uparrow}_{top}$	Absorber
0- 340			
line-by-line	40.35	32.21	H_2O (*line*)
Parameterization	40.25	32.08	H_2O (*line*)
340- 540			
line-by-line	47.34	52.20	H_2O (*line*)
Parameterization	47.16	51.97	H_2O (*line*)
540- 800			
line-by-line	53.54	51.13	H_2O (*line*, *continuum*), CO_2
Parameterization	51.73	51.40	H_2O (*line*, *continuum*), CO_2
800- 980			
line-by-line	1.46	32.85	H_2O (*line*, *continuum*), O_3
Parameterization	1.61	32.84	H_2O (*line*, *continuum)*
980-1100			
line-by-line	3.13	11.01	H_2O (*line*, *continuum*), O_3
Parameterization*	3.37	10.59	H_2O (*line*, *continuum), O_3*
1100-1215			
line-by-line	1.06	9.97	H_2O (*line*, continuum), O_3
Parameterization	0.97	10.25	H_2O (*line*, *continuum)*
1215-1380			
line-by-line	4.61	8.62	H_2O (*line*, *continuum*)
Parameterization	4.86	8.60	H_2O (*line*, *continuum*)
1380-1900			
line-by-line	10.10	5.01	H_2O (*line*)
Parameterization	10.19	5.09	H_2O (*line*)
1900-3000			
line-by-line	0.42	1.37	H_2O (*line*)
Parameterization	0.44	1.38	H_2O (*line*)
Total			
line-by-line	162.01	204.37	
Parameterization	161.09	204.21	

* The absorption due to O_3 in Bands 4 and 6 are folded into the O_3 absorption tables of this band , see Equation (4.18).

There are a total of 13 minor absorption bands included in the *LW* code (see Table 1). These absorption bands are important in studying the greenhouse climatic effect due to human activities. Table 16 shows the effect of these bands on the fluxes at the top of the atmosphere and the surface. It is the difference between the flux with all the minor bands included and the flux with the absorption due to a given trace gas excluded. The concentration of these trace gases used is 0.28 *ppmv* for N_2O, 1.75 *ppmv* for CH_4, 0.3 *ppbv* for *CFC11*, 0.5 *ppbv* for *CFC12*, 0.2 *ppbv* for *CFC22*, and 350 *ppbv* for CO_2. The effect of these bands is a reduction of the outgoing longwave radiation at the TOA by 2.5 - 5.0 Wm^{-2} and an enhancement of the downward longwave radiation at the surface by ~3 Wm^{-2}.

Table 16. Effects of the minor absorption bands on the fluxes at the top of the atmosphere $\Delta F^{\uparrow}_{top}$ and the surface $\Delta F^{\downarrow}_{sfc}$ as calculated using the LW radiation parameterization. See the text for the gas concentrations used in flux calculations. Units of the fluxes are Wm^{-2}.

	CH_4	N_2O	*CFC's*	*Minor* CO_2	*Total*
			Mid-Latitude Summer		
$\Delta F^{\uparrow}_{top}$	-2.22	-1.83	-0.47	-0.38	-4.91
$\Delta F^{\downarrow}_{sfc}$	+0.86	+0.58	+0.39	+0.86	+2.68
			Sub-Arctic Winter		
$\Delta F^{\uparrow}_{top}$	-1.00	-1.10	-0.19	-0.07	-2.36
$\Delta F^{\downarrow}_{sfc}$	+1.21	+1.23	+0.39	+0.37	+3.20

11. CONCLUDING REMARKS

This technical memorandum documents the *LW* radiation code developed at the Climate and Radiation Branch, NASA/Goddard Space Flight Center, which has been implemented in a number of cloud, weather, and climate models. This code includes all the major absorbers and most of the minor absorbers. Cloud optical properties are computed as functions of the ice/liquid water content, the effective particle size, and spectral bands. Aerosol optical properties are specified as input to the code. Scattering due to clouds and aerosols is included by scaling the optical thickness. To enhance the accuracy and speed of flux calculations, different approaches have been applied to different spectral bands for transmission calculations. In the vertical integration of fluxes, the upward emission and downward emission of a layer, including clouds, are separately computed in order to achieve a high degree of accuracy. Sample calculations show that this code can compute accurately fluxes and cooling rate within 1% and 0.15 C/day (0.25 ˚C/day in the stratosphere), respectively, of the line-by-line calculations.

Depending upon the purpose of the *LW* flux calculations and the nature of the atmospheric model, there are a number of options available for efficiently running this code;

1. When the upper stratosphere is not crucial in a study, one can choose the option high=.false. In this case, cooling rate in the upper stratosphere above the 10-hPa level is greatly underestimated. When one chooses high=.true., the cooling rate is computed accurately from the surface to the 0.01-*hPa* level, but the computation is slower.

2. When the absorption in the minor bands (N_2O, CH_4, *CFC's*, and minor CO_2) are not important in certain studies, one can choose trace=.false. The absorption due to those bands is not included.

3. When a vegetation layer is added, the emission and reflection of both the ground and the canopy are included in computing the radiation emitted and reflected by the combined vegetation-ground surface. Set vege=.true. if a vegetation layer is included.

4. For many cloud and meso-scale models, the size of a grid box is small. Factional cloud cover of a layer is either 0 or 1. Treatment of overlapping of clouds at different layers is not an issue, and the option overcast=.true. can be used to reduce computing time.

5. The cloud optical thickness either can be computed from the cloud ice/liquid water content and the effective mean particle size or can be an input to the *LW* code. Set cldwater=.true. for the former and cldwater=.false. for the latter,

6. Set aerosol=.true. if aerosols are included in computing atmospheric transmission functions. Otherwise set aerosol=.false.

There are still rooms for improvement to the code especially the parameterization for cloud optical thickness and the overlapping among cloud layers. To be available for use by atmospheric researchers, we have put this code and the documentation at *http://climate.gsfc.nasa.gov/~chou/clirad_lw*. They will be updated with new developments of the parameterization.

ACKNOWLEDGMENT

This work was supported by the Global Atmospheric Modeling and Analysis Program, Office of Earth Science, NASA Headquarters.

REFERENCES

Arking, A., and K. Grossman, 1972: The influence of line shape and band structure on temperatures in planetary atmospheres. *J. Atmos. Sci.*, **29**, 937-949.

Bacmeister, J. T., and M. J. Suarez,, 2001: Wind-stress simulations and equatorial dynamics in an AGCM. Part I: Basic results from a 1979-1999 forced SST experiment. *J. Atmos. Sci.*, **58**.

Chou, M.-D., and A. Arking, 1980: Computation of Infrared Cooling Rates in the Water Vapor Bands. *J. Atmos. Sci*., **37**, 855-867.

Chou, M.-D., and L. Kouvaris, 1991: Calculations of Transmission Functions in the IR CO_2 and O_3 Bands. *J. Geophys. Res*., **96**, 9003-9012.

Chou, M.-D, and M. Suarez, 1994: An efficient thermal infrared radiation parameterization for use in general circulation models. *NASA Tech. Mem. 104606*, **3**, Technical Report Series on Global Modeling and Data Assimilation. 85 pp.

Chou, M.-D, and M. Suarez, 2002: A solar radiation parameterization for atmospheric studies. *NASA Tech. Memo*. 104606, Vol. 15, 40 pp.

Chou, M.-D., W. Ridgway, and M.-H. Yan, 1993: One-Parameter Scaling and Exponential-Sum Fitting for Water Vapor and CO_2 Infrared Transmission Functions. *J. Atmos. Sci.*, **50**, 2294-2303.

Chou, M.-D., K.-T. Lee, S.-C. Tsay, and Q. Fu, 1999: Parameterization for cloud longwave scattering for use in atmospheric models. *J. Climate*, **12**, 159-169.

Chou, M.-D., M. J. Suarez, C. H. Ho, M. M. H. Yan, and K. T. Lee, 1998: Parameterizations for cloud overlapping and shortwave single-scattering properties for use in general circulation and cloud ensemble models. *J. Climate*, **11**, 202-214.

Clough, S. A., F. X. Kneizys, and R. W. Davies, 1989: Line shape and the water vapor continuum. *Atmos. Res*., **23**, 229-241.

Fu, Q, and K.-N. Liou, 1992: On the correlated *k*-distribution method for radiative transfer in nonhomogeneous atmospheres. *J. Atmos. Sci.*, **49**, 2153-2170.

Fu, Q., P. Yang, and W. B. Sun, 1998: An accurate parameterization of the infrared radiative properties of cirrus clouds for climate models. *J. Climate*, **11**, 2223-2237.

Geleyn, J.-F., and A. Hollingsworth, 1979: An economical analytical method for the computation of the interaction between scattering and line absorption of radiation. *Beitr. Phys. Atmos.*, **52**, 1-16.

Goody, R. M., R. West, L. Chen, and D. Crisp, 1989: The correlated-*k* method for radiation calculation in nonhomogeneous atmospheres. *J. Quant. Spectrosc. Radiat. Transfer*, **42**, 539-550.

Harshvardhan, D. A. Randall and T. G. Corsetti, 1987: A fast radiation parameterization for atmospheric circulation models. *J. Geophy. Res.*, **92**, 1009-1016.

Kratz, D. P., M.-D. Chou, and M. M.-Y. Yan, 1993: Infrared radiation parameterizations for the minor CO_2 bands and for several *CFC* bands in the window region. *J. Climate*, **6**, 1269-1281.

Kratz, D. P., M.-D. Chou, M. M.-H. Yan, and C.-H. Ho, 1998: The *k*-distribution method for computing climate radiative forcing due to minor trace gases. *J. Geophy. Res.*, **103**, 31647-31656.

Lacis, A., and V. Oinas, 1991: A description of the correlated *k*-distribution method for modeling nongray gaseous absorption, thermal emission, and multiple scattering in vertically inhomogeneous atmospheres. *J. Geophy. Res.*, **96**, 9027-9063.

Li, J., 2000: Accounting for overlap of fractional cloud in infrared radiation. *Q. J. R. Meteor. Soc*., **126**, 3325-3342.

Liang, X.-Z., W.-C. Wang, 1997: Cloud overlap effects on general circulation model climate simulations. *J. Geophy. Res.*, **102**, 11039-11047.

Manabe, S., and R. E. Strickler, 1964: Thermal equilibrium of the atmosphere with a convective adjustment. J. *Atmos. Sci*., **21**, 361-385.

McClatchey, R. A., R. W. Fenn, J. E. A. Selby, F. E. Volz and J. S. Garing, 1972: Optical properties of the atmosphere, *3rd ed. AFCRL*-72-0497, 108 pp.

McFarquhar, G. M., 2000: Comments on 'Parameterization of effective sizes of cirrus-cloud particles and its verification against observations' by Zhian Sun and Lawrie Rikus. *Q. J. R. Meteorol. Soc.*, **126**, 1-5.

Mlawer, E. J., S. J. Taubman, P. D. Brown, M. J. Iacono, and S. A. Clough, 1997: Radiative transfer for inhomogeneous atmospheres: RRTM, a validated correlated-*k* model for the longwave. *J. Geophy. Res.*, **102**, 16663-16682.

Raisanen, P., 1998: Effective longwave cloud fraction and maximum-random overlap of clouds: A problem and a solution. *Mon. Wea. Rev.*, **126**, 3336-3340.

Roberts, R. E., J. E. A. Selby and L. M. Biberman, 1976:: Infrared continuum absorption by atmospheric water vapor in the 8-12 μm window. *Appl. Opt.*, **15**, 2085-2090.

Rothman, L. S., and co-authors, 1998: The HITRAN molecular spectroscopic database and HAWK (HITRAN Atmospheric Workstation): 1996 Edition. *J. Quant. Spectrosc. Radiat. Transfer*, **60**, 665-710.

Sud, Y., and D. M. Mocko, 1999: New snow-physics to complement SSiB. Part I: Design and evaluation with ISLSCP initiative I datasets. *J. Meteor. Soc. Japan*, **77**, 335-348.

Szczodrak, M., P. H. Austin, and P. B. Krummel, 2001: Variability of optical depth and effective radius in marine strtocumulus clouds. . *J. Atmos. Sci*,, **58**, 2912-2926.

Tao, W.-K., J. Simpson, D. Baker, S. Braun, M.-D. Chou, B. Ferrier, D. Johnson, A. Khain, S. Lang, B. Lynn, C.-L. Shie, D. Starr, C.-H. Sui, Y. Wang and P. Wetzel, 2001: Microphysics, radiation and surface processes in a non-hydrostatic model, *Meteor. and Atmos. Phys.* (submitted).

Wang, W.-C., and G. Y. Shi, 1988: Total band absorptance and k-distribution function for atmospheric gases. *J. Quant. Spectrosc. Radiat. Transfer*, **39**, 387-397.

Wu, M.-L. C., 1980: The exchange of infrared energy in the troposphere. *J. Geophy. Res.*, **85**, 4084-4090.